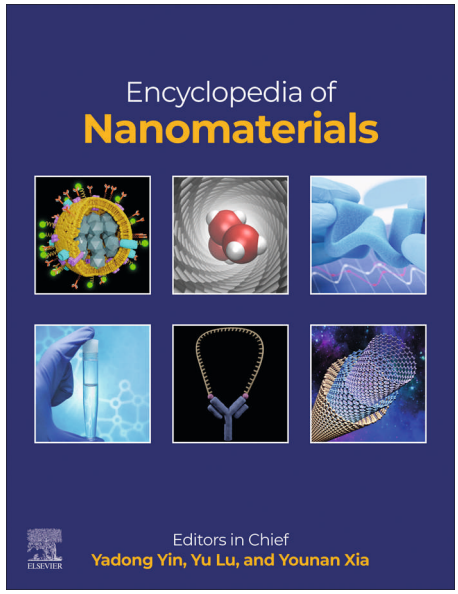

Duan, Hanyi, Lin, Yao and He, Jie (2023) Metal nanoparticles grafted with polymeric ligands: Self-assembly guided by polymers in solution. In: Yadong Yin, Yu Lu and Younan Xia (eds.) *Encyclopedia of Nanomaterials,* vol. 2, pp. 390–406. Oxford: Elsevier.

http://dx.doi.org/10.1016/B978-0-12-822425-0.00004-X

Metal nanoparticles grafted with polymeric ligands: Self-assembly guided by polymers in solution

Hanyi Duan, Polymer Program, Institute of Materials Science, University of Connecticut, Storrs, CT, United States
Yao Lin and Jie He, Polymer Program, Institute of Materials Science, and Department of Chemistry, University of Connecticut, Storrs, CT, United States.

Abstract

Grafting polymer ligands on metal nanoparticles not only offers new solutions to resolve the colloidal stability of metal nanoparticles, but also provides new opportunities to control over the interparticle interaction and therefore the self-assembly nanostructure of metal nanoparticles. We summarize the recent advances in synthesis, surface chemistry and self-assembly of metal nanoparticles grafted by synthetic polymer with an emphasis on polymer-grafted plasmonic nanoparticles.

Graphical Abstract

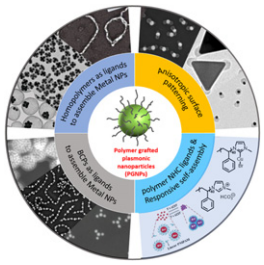

Key Points

- Design of polymer ligands with new binding motifs.
- Ligand exchange methods of metal nanoparticles using synthetic polymers.
- Template synthesis of metal nanoparticles using polymers.
- Polymer-guided self-assembly of metal nanoparticles.
- Responsive self-assembly of metal nanoparticles.

Introduction

Metal nanoparticles (NPs) tend to aggregate in solution like other colloidal dispersions in the absence of surface ligands (Shaw, 1980). Upon aggregation, metal NPs would lose many of their unique properties related to nano-effects. The aggregation is usually caused by the strong, unregulated interparticle attraction, like van der Waals interaction. Adding capping ligands on the surface of metal NPs to counteract such interparticle attraction can stabilize colloidal metal NPs in solution. Capping ligands offset the interparticle attraction mostly through a relatively long-range interaction, like electrostatic repulsion. Common molecular capping

ligands, such as oleic amine, (Leff *et al.*, 1996) oleic acid, (Zhang *et al.*, 2006) citrate, (Frens, 1973) and cetrimonium bromide (CATB), (Jana *et al.*, 2001) have been broadly used in control synthesis of various metal NPs. Capping ligands provide a strong solvation of metal NPs in various solvents like water and other organic solvents. Those ligands define the surface properties of metal NPs in solution. For example, gold NPs (AuNPs) capped with CATB are water-soluble; while AuNPs capped with oleic amine can be dispersed in non-polar solvents, like hexane and toluene; even though they have identical core-forming materials. Therefore, the surface ligands determine their interfaces with solvents. However, the stability provided by capping ligands is usually limited. Metal NPs capped with CTAB or citrate become unstable in the presence of electrolyte due to the disruption of the electrical double layer (Ojea-Jiménez and Puntes, 2009). In some other scenarios, colloidal stability alone is not sufficient. For example, when metal NPs are used in a biological environment, protein adsorption can cause the loss of biological function of NPs even without significant aggregation (Larson *et al.*, 2012). Therefore, surface ligands are of key importance to determine the function and properties of metal NPs (Mout *et al.*, 2012).

Polymer ligands can provide superior stability to metal NPs in comparison to small molecular ligands. First of all, the size of polymer ligands is comparable with that of commonly used metal NPs. The chain length of polymer ligands or the end-to-end distance is in the range of 5–50 nm depending on the molecular weight of polymers. Polymer ligands when bound to the surface of metal NPs offer a sizable buffer zone to overcome undesired van der Waals interaction between NPs. The polymer layer also provides a sterically repulsive interface because of highly solvated polymer chains (or referred as "osmotic repulsion") (Tadros, 2013). With polymer ligands like polyvinylpyrrolidone (PVP) (Koczkur *et al.*, 2015) and thiol-terminated poly(ethylene oxide) (PEO-SH), (Gao *et al.*, 2012a) AuNPs can be stabilized in water containing electrolytes, acid/base, organic solvents and/or biological media. Second, polymers as surface ligands endow new surface properties and functionalities to metal NPs. PEO and other hydrophilic polymers when grafted on metal NPs can form a large, hydrated shell to reduce nonspecific protein adsorption, (Gal *et al.*, 2018) which is essential for the *in-vivo* use of NPs as nanomedicines. Polymer ligands can be readily functionalized with biological molecules of interest by taking advantage of abundant reactive sites on polymers for specific conjugation reactions (Liu and Thierry, 2012). With the suitable polymer ligands, metal NPs can stabilize surface-bound biological molecules, (Delong *et al.*, 2010) *e.g.*, proteins and nucleotide acids. Third, polymers can make metal NPs become "smart" in response to external stimuli. When modified by small molecular ligands, the surface properties are fixed with a specific type of ligands. In contrast, polymer ligands allow for a broad range of responsiveness to metal NPs that cannot be easily realized by small molecular ligands. For example, hydrophobicity of metal NPs can be varied by a stimulus that switches the physicochemical state of polymer ligands, *i.e.*, hydrophilic-to-hydrophobic transition. Such responsiveness can dynamically change the solubility of metal NPs in different solvents (Sánchez-Iglesias *et al.*, 2018) or provide control over the surface accessibility of metal NPs (Chen *et al.*, 2019).

As surface ligands, polymers offer additional switches to control the properties of metal NPs (Moffitt, 2013; Liu *et al.*, 2010; Yi *et al.*, 2020a; Yi *et al.*, 2020b; Duan *et al.*, 2020). Among many unique properties of metal NPs, localized surface plasmon resonance (LSPR) is of particular interest. As the collective oscillation of free electrons on the NP surface resonates with incident light, the LSPR leads to a strong resonance absorption at a specific wavelength. While the LSPR absorption is characteristic for individual metal NPs with distinctive size, shape, composition, and surface environment, the plasmonic field of metal NPs in close proximity can couple (Jain *et al.*, 2007). The plasmon coupling usually leads to the shift of the LSPR absorption or the yield of the new resonance peaks distinct from individual NPs. The interparticle plasmon coupling is highly distance-dependent. In the assemblies of polymer-grafted plasmonic NPs (PGNPs), polymer ligands act as a passive and non-conductive coating layer, dominant the interparticle distances and thereafter plasmon coupling of metal NP cores (Nie *et al.*, 2007; Li *et al.*, 2015). For PGNPs, the self-assembly of PGNPs can be triggered by varying polymer-polymer and polymer-solvent (or media broadly) interactions. In solution, PGNPs with hydrophobic polymer ligands can assemble in water, as driven by hydrophobic interaction. For example, spherical AuNPs capped with citrate have a plasmon resonance peak around 520 nm. After grafted by thiol-terminated polystyrene (PS-SH), those AuNPs can assemble in water as driven by the hydrophobicity of PS. Those PGNPs usually show a red shift of their plasmon resonance peak to the range of 540–580 nm (Sánchez-Iglesias *et al.*, 2012). In the assembly of larger AuNPs ($\sim$40 nm in diameter), the stronger plasmon coupling can further shift the resonance peak of their assemblies to 700–800 nm. In solid state, PGNPs can co-assemble with a block copolymer (BCP) where the microphase separation of the BCP can template the organization of metal NPs due to their unfavorable mixing entropy (Li *et al.*, 2011; Kao *et al.*, 2012; Kim *et al.*, 2006). The organization of PGNPs within the nano-confined polymer domains may result in interesting optical coupling over space, *e.g.*, chiral plasmon resonance (Liang *et al.*, 2014).

This article focuses on the synthesis, surface chemistry and self-assembly of metal NPs grafted by synthetic polymer with an emphasis on PGNPs with the core of plasmonic AuNPs and silver NPs (AgNPs). We started with the synthetic strategies, including so-called "grafting to" and "grafting from" approaches, to attach polymer ligands on metal NPs ("Section Grafting Polymer Ligands on Metal NPs"). We outlined the challenges to design and develop novel anchoring groups and precisely control the numbers and densities of polymer ligands. The isotropic-to-asymmetric surface patterning and the programmable self-assembly of those PGNPs are highlighted in "Section Anisotropic Surface Patterning of PGNPs". We further introduced the self-assembly of PGNPs grafted by homopolymer ("Section Homopolymers as surface ligands to assemble metal NPs in solution") or BCP ligands ("Section BCPs as ligands to guide the self-assembly of metal NPs") together with their unique collective plasmonic properties. Finally, some of the novel designs on stimuli-responsive PGNP assemblies with fully reversible plasmonic coupling and fast colorimetric response are highlighted in "Section Responsive self-assembly of metal nanoparticles". We apologize if some important works that have not been cited here as the article does not serve as a comprehensive literature survey.

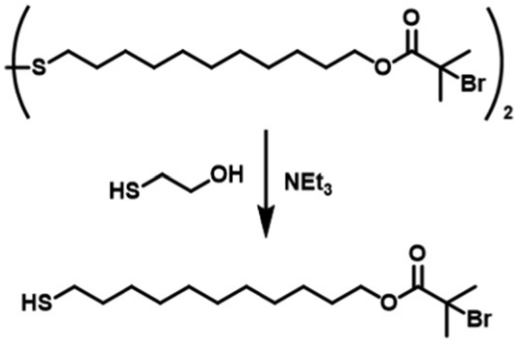

Fig. 1 Synthesis of the thiol-terminated ATRP initiator-2,2′-dithiobis[1- (2-bromo-2-methylpropionyloxy)]ethane (DTBE). Redrawn from Nuß, S., Böttcher, H., Wurm, H., Hallensleben, M.L., 2001. Gold nanoparticles with covalently attached polymer chains. Angew. Chem. Int. Ed. 40, 4016–4018.

Grafting Polymer Ligands on Metal NPs

Capping ligands of metal NPs can be replaced by synthetic polymers through ligand exchange. We categorize synthetic polymer ligands based on their anchoring groups. Weak anchoring groups such as COOH, OH and O=C−N are very labile and their binding to NPs is dynamic. Polymers with many weak anchoring groups can "wrap" the surface of metal NPs through multiple binding sites (Kyrychenko *et al.*, 2015). Those polymer ligands are usually water-soluble and commercially available, like poly(acrylic acid) (PAA), poly(N-vinyl-2-pyrrolidone) (PVP) and poly(vinyl alcohol) (PVA). PVP, for example, has been broadly used as ligands in synthesis of AuNPs (Gao *et al.*, 2012b) and Ag nanocubes/nanowires, (Koczkur *et al.*, 2015; Sun *et al.*, 2002) taking advantage of the weak coordination between its carbonyl group and metal atom. Given many repeating units, the polymer chains entangle and wrap around the surface of metal NPs. Although metal NPs grafted by those polymers are reasonably stable against electrolytes or even under elevated temperature, the grafting process is not so well controlled in terms of the number density and the functionality of polymers.

Polymer ligands can be anchored on metal NPs through other anchoring groups like thiols and N-heterocyclic carbenes (NHCs). Those anchoring groups bind strongly with a broad range of metals, and the binding is less dynamic as compared to those weak anchoring groups. For example, the binding energy of Au–S and Au-C is ∼126 and ∼158 kJ mol^{-1}, respectively, which are close to the strength of the strongest hydrogen bonds (Lavrich *et al.*, 1998; Crudden *et al.*, 2014; Engel *et al.*, 2017). The structural features of those strong anchoring groups are similar to their organometallic complexes. For example, thiols bind with Au through the formation of Au-thiolate commonly referred as Au-S-Au on the bridge site. Adatom-bound motifs, like S-Au (I)-S and S-Au (I)-S-Au (I)-S, are also seen on the surface of nanoclusters since surface metal atoms are often found in their oxidative states (Häkkinen, 2012). NHCs that are usually larger than thiolate can bind on the atop sites (Narouz *et al.*, 2019). Those two anchoring groups form stable self-assembled monolayers (SAMs) on the surface of various metals (Crudden *et al.*, 2014; Bain *et al.*, 1989; Han *et al.*, 2001; Yamamoto *et al.*, 1993; Bakker *et al.*, 2020). Polymers with those strong anchoring groups could be added to the surface of metal NPs as polymer brushes as one end of polymer ligands is tethered on the surface of metal NPs while polymer chains are extended away from the surface.

Grafting polymer ligands with strong anchoring groups on metal NPs can be achieved through "grafting from" and "grafting to" methods. In both approaches, ligand exchange is first carried out to replace the capping agents with active molecules to grow polymers subsequently (grafting from) or to tether with polymer ligands directly (grafting to). In the grafting from approach, small molecules with anchoring groups like thiols are first introduced to the surface of metal NPs. Those small molecules can either initiate polymerization (*e.g.*, atom transfer radical polymerization, ATRP) or transfer radicals (*e.g.*, reversible addition−-fragmentation chain-transfer polymerization, RAFT) to grow polymer chains. In case of ATRP, small molecular ligands are designed with a thiol or disulfide at one end and a tertiary halide at the other end (see **Fig. 1**) (Nuß *et al.*, 2001). Those ligands can be added to metal NP, *e.g.*, AuNPs *via* ligand exchange (Nuß *et al.*, 2001) or *in situ* synthesis (Roth and Theato, 2008; Ohno *et al.*, 2002). Further polymerization will only be initiated from the tertiary halide end to form polymers tethered on the surface of metal NPs. In case of poly(methyl methacrylate) (PMMA, 25 kg/mol) on AuNPs, the ligand density around 0.3 chains/nm^2 was reported by Ohno *et al.* (2002) For poly(N-Isopropylacrylamide) (PNIPAM, 9.5 kg/mol) grafted AuNPs, the ligand density around 2.2 chains/nm^2 was reported by Roth *et al.* (Roth and Theato, 2008).

One drawback of the "grafting from" method is the upper limit of NP sizes. Since the molecular ligands are usually short (C_{12}∼C_{18}), they can only stabilize AuNPs less than 5 nm. Combing the two grafting methods, *i.e.*, grafting from and grafting to, has been demonstrated by Duan and coworkers to grow polymer chains on large AuNPs ∼14 nm (Song *et al.*, 2011; Cheng *et al.*, 2010). To provide the stability of AuNPs, the ligand exchange was carried out using a binary mixture of PEO-SH (5 kg/mol) and 2,2′-dithiobis[1-(2-bromo-2-methylpropionyloxy)]ethane (DTBE, **Fig. 1**). Those modified AuNPs supported the growth of PMMA (22 kg/mol) and poly(2-(diethylamino)ethyl methacrylate) (PDEA) *in-situ* with PEG to form amphiphilic AuNPs. The overall ligand density reached 0.43 chains/nm^2.

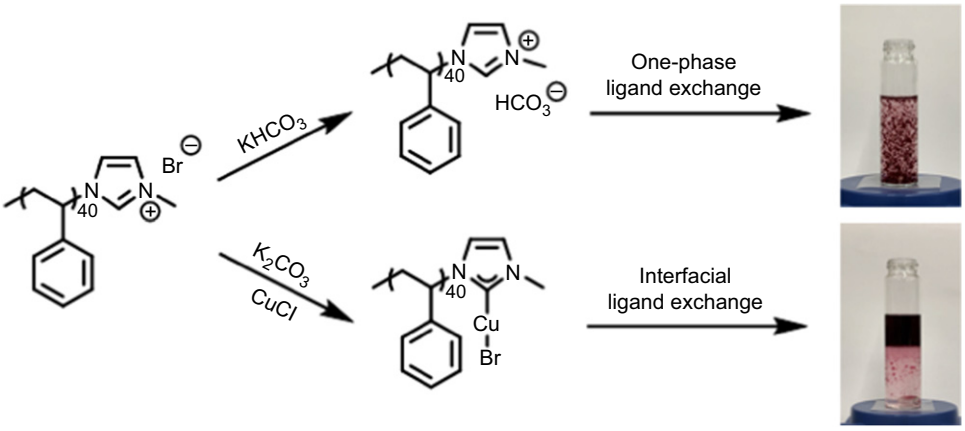

Fig. 2 Synthesis of two polymer NHC precursors through the end group functionalization of bromide-terminated PS_{40} and the subsequent surface modification of AuNPs through ligand exchange. Cited from Zhang, L., Wei, Z., Meng, M., Ung, G., He, J., 2020. Do polymer ligands block the catalysis of metal nanoparticles? Unexpected importance of binding motifs in improving catalytic activity. J. Mater. Chem. A 8, 15900–15908.

In the "grafting to" method, end-functionalized polymers with desired molecular weights and functionality are synthesized first before grafting to metal NP *via* ligand exchange. Since polymer ligands carry large steric hindrance during ligand exchange, the grafting to method usually produces polymer brushes with a slightly lower grafting density as compared to the grafting from method. Nevertheless, the grafting to method allows the use of pre-designed metal NPs with well-defined nanostructures and the utilization of the large library of metal NPs with different shapes, sizes and chemical composition, usually not accessible to the grafting from method. Synthesis at a small scale (μg to mg of metal NPs) is possible, which is beneficial when working with precious metals like Au and Pt. The thiol-terminated polymers can be synthesized using anionic polymerization or RAFT polymerization. In particular, RAFT polymerization can be carried out under mild conditions and the dithioester or trithioester end group can be reduced to produce thiol-terminated polymers (Ebeling and Vana, 2013; Lowe *et al.*, 2002; Wang *et al.*, 2021). Additionally, PS-SH as one of the most broadly used polymer ligands is commercially available.

The grafting to modification can be carried out in one-phase or biphasic ligand exchange. In one-phase ligand exchange, thiol-terminated polymers and metal NPs are mixed in one solvent as a good solvent to dissolve polymers and disperse NPs. For example, water-solution AuNPs capped with citrate can be dispersed in dimethylformamide (DMF), acetone and tetrahydrofuran (THF) in the presence of PS-SH, or in water for PEG-SH. Oleate-capped AuNPs can be dispersed in THF and toluene even in the absence of PS-SH (Zhang *et al.*, 2020). To avoid the precipitation of polymers, as-synthesized AuNPs are usually pre-concentrated to remove most of the nonsolvent of polymers (Goulet *et al.*, 2012). The ligand exchange usually takes 12–24 h to reach a reasonable grafting density to stabilize NPs. The grafting density of polymers is highly dependent on the molecular weight. PS_{19}-SH (2 kg/mol) reached a grafting density of 0.6 chains/nm^2 while PS_{125}-SH (13.3 kg/mol) only showed a grafting density of 0.04 chains/nm^2 as demonstrated in the pioneering work of Lennox and co-workers (Corbierre *et al.*, 2004). On the other hand, the ligand exchange can be performed at the biphasic interface of water and oil. It is very efficient to transfer small metal NPs (< 3 nm) from water to the oil phase (Brust *et al.*, 1994). With thiol-ended hydrophobic polymers (like PS-SH), the biphasic ligand exchange can readily take place for water-soluble AuNPs at the interface of water-toluene (He *et al.*, 2013b).

Although thiol is the most popular binding motif of polymer ligands, the metal-thiolate binding is subject to the slow oxidation in air (Thanneeru *et al.*, 2020). When thiolate is oxidized to sulfone or sulfoxide, thiol-ended polymer ligands will detach from metal NPs to destabilize PGNPs. The dynamic nature of metal-thiolate binding under elevated temperature may affect the thermal stability of those PGNPs. NHC as a stronger binding motif to metal NPs has received considerable attention since it was first reported by Siemeling and coworkers (Weidner *et al.*, 2011). Metal-carbon bonds resulted from the NHC-metal binding are more robust against oxidation and high temperature, as compared to metal-thiolate. The NHC motif also shows strong σ donation (lone pair in carbon atom to metal) and increases the surface electron density on metal NPs, leading to some unprecedented applications of PGNPs in catalysis and optoelectronics (Zhang *et al.*, 2019; Westmoreland *et al.*, 2020) With the recent effort to resolve the synthetic challenges in polymer NHCs, polymer NHC ligands become available nearly for any polymers synthesized from ATRP.

He and coworkers demonstrated the conversion of polymers terminated with halides to polymer NHCs (**Fig. 2**) (Zhang *et al.*, 2020; Thanneeru *et al.*, 2020; Zhang *et al.*, 2019). Simply, the quaternization of those polymers with methyl imidazole can produce polymers terminated with imidazolium. In one method, the counter ion exchange of imidazolium with $KHCO_3$ can result in the formation of a polymer NHC precursor, *i.e.*, imidazolium-ended polymers with bicarbonate. This family of polymers can modify metal NPs through one-phase ligand exchange. In a typical reaction, PS_{40} ended with imidazolium bicarbonate could be directly injected into the aqueous solution of AuNPs under stirring. The PS NHC modified AuNPs would crush out within 2 min since water is a nonsolvent for PS. In such process, the bicarbonate as a weak base can deprotonate imidazolium to form NHCs that bind with AuNPs even in the presence of water. In another method, imidazolium-terminated polymers can be converted to

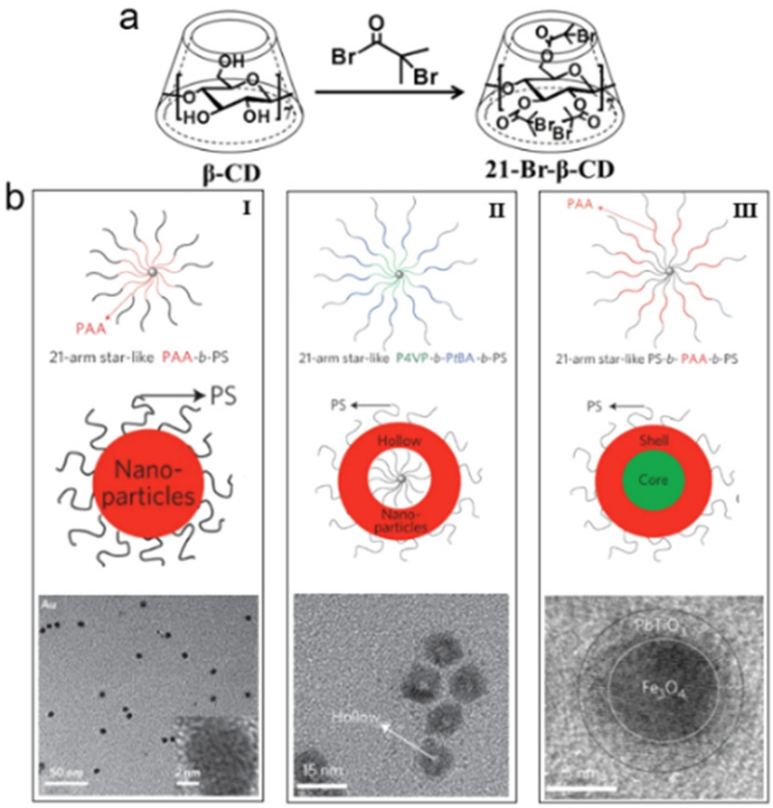

Fig. 3 (a) Synthesis of 21-armed β-CD ATRP initiator. (b) Chemical structure of different star-like block polymer templates and the corresponding nanoparticles (I: spherical AuNPs; II: hollow AuNPs; III: core-shell Fe_3O_4-$PbTiO_3$ NPs). Cited from (a) Chen, Y., Wang, Z., He, Y., *et al.*, 2018. Light-enabled reversible self-assembly and tunable optical properties of stable hairy nanoparticles. Proc. Natl. Acad. Sci. USA 115, E1391–E1400. (b) Pang, X., Zhao, L., Han, W., Xin, X., Lin, Z., 2013. A general and robust strategy for the synthesis of nearly monodisperse colloidal nanocrystals. Nat. Nanotechnol. 8, 426–431.

NHC-Cu (I)-terminated polymers in the presence of CuCl and K_2CO_3 as the weak base. For example, PS_{40} terminated NHC-Cu (I) (1 mg/mL) could modify AuNPs using biphasic ligand exchange at the interface of toluene and water. Citrate-capped AuNPs could be transferred from water to toluene containing PS_{40} terminated NHC-Cu (I) after stirring for 4 min. The two polymer NHC precursors could complete the ligand exchange within 5 min, much more efficient as compared to thiol-terminated polymer ligands. The grafting density was 0.35 chains/nm^2 and 0.29 chains/nm^2 for imidazolium-terminated PS_{40} with bicarbonate and PS NHC-Cu (I), respectively (Zhang *et al.*, 2020).

Other than ligand exchange, polymer ligands can be added to metal NPs through template synthesis. Template synthesis uses the nanostructures of polymer assemblies or macromolecular architectures to grow metal NPs *in situ*. Earlier studies show that reverse micelles of amphiphilic BCPs like polystyrene-*b*-poly(2-vinylpyridine) (PS-*b*-P2VP) could bind metal ions in the P2VP core stabilized by the PS corona (Mössmer *et al.*, 2000; Spatz *et al.*, 2000). After reduction, metal NPs would covalently link to the PS corona that formed a brush layer as surface ligands. The pioneering works by Eisenberg *et al.* demonstrated the growth of CdS NPs using the reverse micelles of polystyrene-*b*-poly(acrylic acid) (PS-*b*-PAA) (Moffitt *et al.*, 1995). More recently, Lin's group has developed a general methodology to *in situ* synthesize PGNPs using template synthesis of brush polymers (Liu *et al.*, 2020). Star-shaped brush polymers grown on a 21-armed β-cyclodextrin (β-CD) can be used as a universal template to grow spherical, core-shell and hollow metal NPs (Pang *et al.*, 2013). For example, with the 21-armed β-CD as an initiator (**Fig. 3**(a)), polystyrene-*b*-poly(*tert*-butyl acrylate) (PS-*b*-PtBA) could be grown with subsequent hydrolysis to PS-*b*-PAA (**Fig. 3**(b)). Those brush polymers formed unimolecular spherical micelle in the selective solvent of PS (*e.g.*, the mixing solvent of DMF and benzyl alcohol, DMF/BA=9/1) where metal precursors only coordinated to the PAA core. The size of those NPs could be controlled by adjusting the molecular weight of the PAA block. This strategy could be easily extended to the synthesis of various NPs like AuNPs, AgNPs, Fe_3O_4, CdSe, $PbTiO_3$ and TiO_2. Core-shell and hollow nanoparticles could be synthesized using a similar approach by adjusting the chemical composition and the sequence of star-shaped BCPs (**Fig. 3**(b)). The same strategy was applied to the cellulose based BCP templates to grow 1-D plasmonic nanorods and nanotubes (Pang *et al.*, 2016). As compared to those NPs prepared from ligand exchange, those PGNPs are unique in terms of their ligand chemistry. With covalent linkage, the surface ligands are not dynamic in nature anymore and therefore very stable even under extensive thermal annealing.

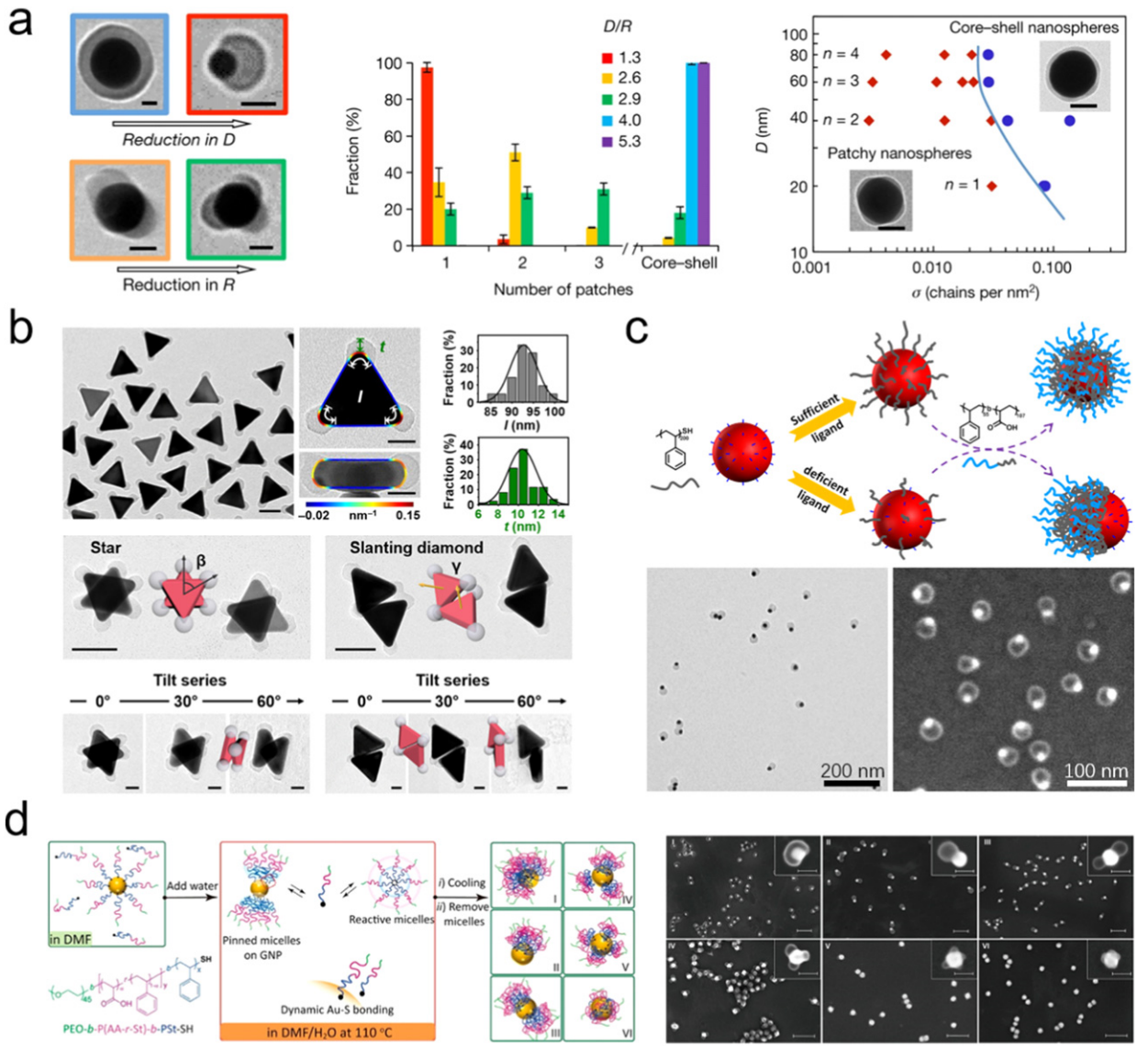

Fig. 4 (a) Polymer patches formation on the PS grafted AuNPs. The number of patches is dependent on the nanoparticle size, polymer chain length and grafting density. (b) Formation of tip-patched nanoprisms and their self-assemble behavior. (c) Scheme of surface patterning of AuNPs: core-shell and Janus type PGNPs. (d) Schematic representation of copolymer micelle patches formation and SEM (inset: high magnification) images of the representative patches AuNPs. Cite from (a) Choueiri, R.M., Galati, E., Thérien-Aubin, H., *et al.*, 2016. Surface patterning of nanoparticles with polymer patches. Nature 538, 79–83. (b) Kim, A., Zhou, S., Yao, L., *et al.*, 2019. Tip-patched nanoprisms from formation of ligand islands. J. Am. Chem. Soc. 141, 11796–11800. (c) Duan, H., Luo, Q., Wei, Z., Lin, Y., He, J., 2021. Symmetry-broken patches on gold nanoparticles through deficient ligand exchange. ACS Macro Lett. 10, 786–790. (d) Yang, Y., Yi, C., Duan, X., *et al.*, 2021. Block-random copolymer-micellization-mediated formation of polymeric patches on gold nanoparticles. J. Am. Chem. Soc. 143, 5060–5070.

Anisotropic Surface Patterning of PGNPs

Adding polymer ligands to metal NPs through either grafting to or grafting from methods is a kinetically controlled process. In case of grafting to approach, the ligand density usually increases with the reaction time of ligand exchange. Ideally, polymer ligands would replace the capping ligands at a minimum density, (1) to minimize their steric repulsion of adjacent ligands and (2) to avoid the stretching of polymer ligands. To reach a high grafting density, the concentration of polymer ligands in solution is usually 100–1000 times excess than that being grafted. With a high grafting density, dense polymer brushes on NPs form core-shell nanostructures and polymer ligands are evenly distributed to cover metal NPs. Such isotropic distribution of polymer ligands is not always desired because the isotropic interparticle interaction usually leads to the formation of disordered aggregates. Therefore, breaking the symmetry of PGNPs becomes critical in order to control the anisotropic self-assembly of PGNPs rather than disordered clustering.

There are two methods to modify metal NP anisotopically, including site-selective grafting and phase segregation of surface ligands on NPs. Site-selective grafting relies on the different interaction or binding strength of ligands to the surface of metal NP core. This difference can arise from the surface anergy, *e.g.*, Au (111) *vs*. Au (100) for gold nanorods (AuNRs), and/or the unsaturated coordination sites on the surface, e.g., corner and edge sites *vs*. flat surface sites. For example, CTAB-capped AuNRs have surface facets (100) along their longitudinal sides and (111) at the two ends. With CTAB preferentially bound with Au (100) facets, the ligand exchange of AuNRs with PS-SH results in the grafting on (111) facets as demonstrated by Kumecheva's group (Nie *et al.*, 2007). Hydrophilic thiol-ended PEO also shows preferential binding (111) at the two ends of AuNRs and those anisotropic patch polymer ligands can result in the further anisotropic growth of silica on the side of AuNRs (Wang *et al.*, 2013).

Phase segregation of surface ligands has been observed in a mixture of molecular ligands that are thermodynamically unfavorable to mix on the surface of AuNPs, *e.g.*, with different chain lengths (DeVries *et al.*, 2007) and hydrophobicity (Chen *et al.*, 2008). A recent study from Chen's group demonstrated the preferential binding of hydrophobic thiol ligands at the tip of Au nanoprisms (Kim *et al.*, 2019). Au nanoprisms were capped with CTAB and their edge length was 58.9 nm. After adding a hydrophobic ligand such as 2-naphthalenethiols (2-NAT), the modified domain on Au nanoprisms could be identified using polymer micelles of PS-*b*-PAA. During ligand exchange, 2-NAT and PS-*b*-PAA were mixed with nanoprisms in DMF/H_2O. With thermal annealing at 110°C, NAT attached to the prism through Au-S binding and PS-*b*-PAA would collapse on the 2-NAT-covered area due to the hydrophobic interaction between naphthalene and the PS block. The curvature difference between the tip and planar facet of Au nanoprisms led to the selective binding when the 2-NAT concentration was sufficiently low (<1.0 mM). The tip was patched and stabilized by polymer micelles (**Fig. 4**(b)). The thickness and the tip coverage were tuned by adjusting the concentration of PS-*b*-PAA and 2-NAT, respectively. With 2.5 mM of 2-NAT, core-shell nanoprisms fully covered by polymer micelles were generated.

When grafting with hydrophobic polymer ligands, hydrophobicity may drive the phase segregation of surface ligands at a low grafting density. Kumacheva and coworkers studied the phase segregation of PS ligands on the surface of AuNPs (Choueiri *et al.*, 2016). Transferring PS-grafted AuNPs from a good solvent to a poor solvent, *e.g.*, adding water to the DMF solution of PGNPs, would result in the collapse of PS ligands anisotropically. The size of polymer domains was determined by the molecular weight of PS-SH, whereas the number of patches per PGNP was dependent on the relative size of NPs and PS-SH (**Fig. 4**(a)). With 4 vol% of water in DMF, AuNPs (20 nm) grafted with PS (50 kg/mol) at a grafting density of 0.03 chains/nm^2 would form Janus-type polymer patches on the surface of AuNPs. The yield of those asymmetrically coated PGNP reached to 98%. Patch formation was exclusively driven by hydrophobicity of PS ligands. Similar phase segregation was observed using amphiphilic BCP ligands on the surface of AuNPs by He and coworkers (Liu *et al.*, 2017).

The preparation of those asymmetric surface pattering of PGNPs driven by hydrophobicity of polymer ligands is extremely delicate. The formation of patch is limited to a very narrow window of the solvent composition in order to avoid undesired interparticle interaction. Therefore, the separation and isolation of those products are very challenging. He's group recently demonstrated a facial approach to fabricate the symmetry-broken plasmonic AuNPs through the deficient ligand exchange (DLE) (Duan *et al.*, 2021). Since the ligand density was critical to control the phase separation, the concentration of PS-SH ligands was lowered to reach the boundary of phase separation. At the same time, an amphiphilic BCP PS_{55}-*b*-PAA_{107} (M_n = 13.6 kg/mol) was added to stabilize the assembled nanostructure and provide water-solubility of those nanostructures in water (**Fig. 4**(c)). In one-pot ligand exchange, simply mixing citrate-capped AuNPs (13 nm) with PS_{200}-SH and PS_{55}-*b*-PAA_{107} and annealing the mixture at 100°C in DMF/H_2O (21/4) would result in formation of symmetry-breaking surface coating on PGNPs. The ligand grafting density was found to be ~0.1 chains/nm^2 to allow the segregation of polymer ligands. The mechanism behind such structure transitions lied at the interplay of conformation entropy of polymer ligands and the minimization of surface energy. While the collapse and segregation minimized the interface of polymer ligands, the phase segregation avoided the chain compression to stabilize PGNPs.

Nie's group also demonstrated the polymer-micellization-mediated strategy to asymmetrically patch AuNPs grafted with amphiphilic block-random copolymers (Yang *et al.*, 2021). Polymer ligands of PEO_{45}-*b*-P(AA-*r*-St)$_y$-*b*-PS_x-SH (subscript denotes the repeating unit of each block) consisted of hydrophilic PEO tail, a randomly copolymerized middle block and a hydrophobic head to bind AuNPs. The formation of polymer patches on PGNPs was achieved by the thermal annealing of grafted AuNPs in DMF/H_2O mixture at 110 °C. By adjusting the fraction of PS block (f_s = x/ (x + y)) and the water content (C_w), different type of patchy NPs could be generated by the segregation of copolymer ligands (**Fig. 4**(d)). For example, beanlike patch, single patch, and three patches on the surface of 42.4 nm AuNPs were generated at the condition of f_s = 0.76, C_w = 5%; f_s = 0.76, C_w = 10%; and f_s = 0.49, C_w = 20%, respectively. The yield of uniform patchy AuNPs was extremely high, *e.g.*, 94% for beanlike patch, 97.5% for single patch, and 85% for three patches. The dynamic ligand exchange between polymer micelles and grafted AuNPs during thermal treatment was found to be the key for the asymmetric patch of PGNPs as supported by molecular dynamics simulation. The importance of free ligands was also verified by the fact that AuNPs would aggregate under the same condition when the free polymer ligand was removed.

Asymmetric ligand grafting was also realized through template synthesis as demonstrated previously in protected surface modification of colloidal NPs (Xu *et al.*, 2006; Chen *et al.*, 2011). Li and coworkers designed the polymer masking template synthesis to prepare asymmetric coating on AuNPs using polymer single crystal (Wang *et al.*, 2008). PEO-SH (2 kg/mol) could form very uniform lamella single crystals (thickness of 12 nm) in pentyl acetate. Spherical AuNPs (5–6 nm) could be adsorbed and immobilized on the surface of the PEO-SH lamella nanoplates. The exposed surface of AuNPs was then modified with PMMA (30.1 kg/mol, the grafting density of 0.52 polymer chains/nm^2) through the grafting from method. After removal of the PEO-SH template, PGNPs grafted with those two types of polymer ligands asymmetrically could be obtained. Those Janus PGNPs with PEO and PMMA brushes could further self-assemble in dioxane as a poor solvent for PEO to form worm-like aggregates (Wang *et al.*, 2010).

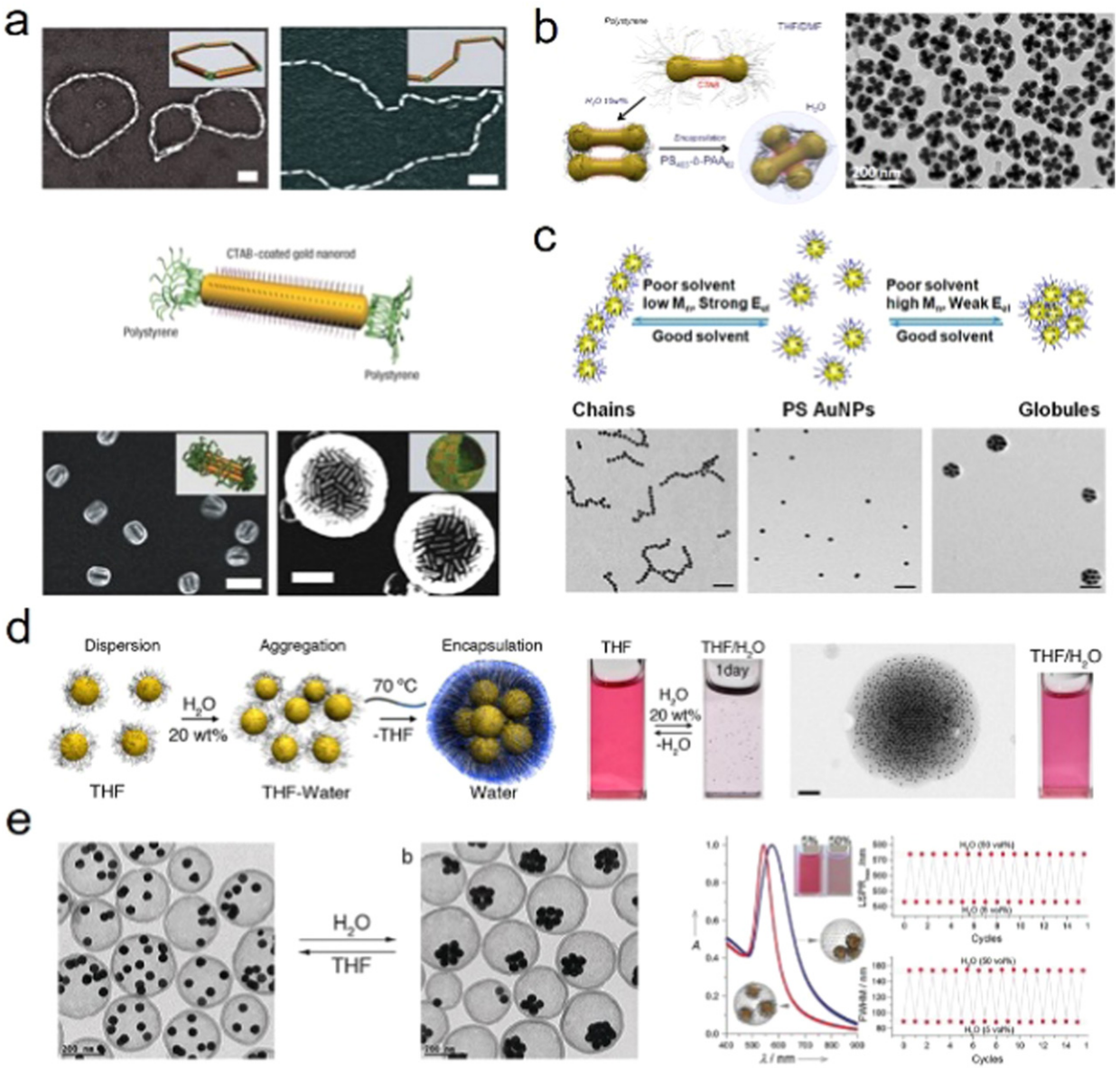

Fig. 5 (a) AuNRs with end grafted PS (middle) and the SEM images of their assemblies (middle) in DMF/H_2O (up) and THF/H_2O (down) mixture with the water content as 6 wt% (left) and 20 wt% (right) (scale bar = 100 nm). (b) Scheme of structure transition from parallel to cross-like arrangement driven by steric effect and the TEM image of cross-like AuNDs dimer. (c) Schematic illustration of the structure transition in AuNPs assemblies and the TEM images of AuNPs chains, individual AuNPs and globules (scale bar = 100 nm). (d) From left to right: scheme of hydrophobicity-driven clustering of PS_{509}-SH capped AuNPs; the corresponding optical image of AuNPs solution before and after clustering; quenching the clustering by the addition of PS_{403}-PAA_{62} (scale bar = 200 nm). (e) TEM images showing the reversible aggregation of 41 nm AuNP capped by PS_{509}-SH inside porous silicon (left) and UV–vis–NIR absorption spectra of capsules during solvent replacement with the evolution of LSPR and FWHM over 15 cycles. Cited from (a) Nie, Z., Fava, D., Kumacheva, E., *et al.*, 2007. Self-assembly of metal–polymer analogues of amphiphilic triblock copolymers. Nat. Mater. 6, 609–614. (b) Grzelczak, M., Sánchez-Iglesias, A., Mezerji, H.H., *et al.*, 2012. Steric hindrance induces crosslike self-assembly of gold nanodumbbells. Nano Lett. 12, 4380–4384. (c) Choueiri, R.M., Klinkova, A., Thérien-Aubin, H.s., Rubinstein, M., Kumacheva, E., 2013. Structural transitions in nanoparticle assemblies governed by competing nanoscale forces. J. Am. Chem. Soc. 135, 10262–10265. (d) Sánchez-Iglesias, A., Grzelczak, M., Altantzis, T., *et al.*, 2012. Hydrophobic interactions modulate self-assembly of nanoparticles. ACS Nano 6, 11059–11065. (e) Sánchez-Iglesias, A., Claes, N., Solís, D.M., *et al.*, 2018. Reversible clustering of gold nanoparticles under confinement. Angew. Chem. Int. Ed. 130, 3237–3240.

Homopolymers as Surface Ligands to Assemble Metal NPs in Solution

As polymer ligands counteract the interparticle van der Waals attraction, the interparticle interaction of PGNPs is mainly steric repulsion as resulted from the solvated polymer ligands in solution. Therefore, the key to assemble PGNPs is to vary the solvation

state of polymer ligands. When the solvent quality for polymers is reduced, the polymer-polymer interaction overwrites the polymer-solvent interaction, leading to the collapse of polymer ligands and the formation of the assembled nanostructures of PGNPs. In case of hydrophobic ligands, hydrophobicity of polymer ligands can drive the self-assembly of grafted metal NPs even with homopolymer ligands. Unlike traditional polymer brushes on NPs, PGNPs can have polymer ligands on specific sites of metal NPs to form anisotropic surface grafting. Kumacheva's group firstly reported the hydrophobicity-driven self-assembly of PS-grafted AuNRs as discussed above (Nie *et al.*, 2007). Those PS-grafted AuNRs analogous to the tri-BCPs could assemble when adding a nonsolvent of PS (**Fig. 5**(a)). In the mixture of DMF/water, the triblocky AuNRs formed chains where the PS tethers at the end of AuNRs collapsed to trigger the end-to-end binding. With 6 wt% of water, the chains of AuNRs grafted with PS_{115}-SH (M_n = 12 kg/mol) enclosed to from rings with an average diameter of 390 nm. In the mixture of THF/water, the side-to-side assemblies of triblocky AuNRs were observed in the forms of bundles and nanospheres. The assembly of AuNRs had a profound impact on the LSPR of nanorods due to the plasmon coupling. The formation of chains and rings led to the red shift (~120 nm) of the longitudinal plasmonic band of AuNRs.

A similar strategy was used to assemble Au nanodumbbells (AuNDs) (Grzelczak *et al.*, 2012). AuNDs were grown from AuNRs as the seed in the presence of excess KI. The iodide could replace the bromide from the end of AuNRs to favor the growth at (111) facets (Grzelczak *et al.*, 2008). With a larger volume at the two ends, PGNPs would have a higher grafting density of PS ligands (PS_{509}-SH, 53 kg/mol) preferentially at the tip of AuNDs owing to the higher surface curvature. When 10 wt% of water was introduced into the DMF/THF (3/1 w/w) solution of PS_{509}-grafted AuNDs, clusters of AuNRs were generated (**Fig. 5**(b)). The blue-shifted longitudinal plasmon band from 910 nm to 885 nm was observed, indicating the assembly of AuNDs in the side-to-side mode. Given the strong steric hindrance between AuNDs as a result of their unique surface curvature, the yield of parallel dimers of AuNDs was 46%. In the presence of a BCP surfactant PS_{403}-*b*-PAA_{62}, the clustering would be quenched as those dimers were encapsulated by polymer micelles. Further increasing the concentration of water would result in a stronger contribution from hydrophobic interaction of polymer ligands. The encapsulated side-to-side dimers were converted to cross-like dimers by thermal treatment (**Fig. 5**(b)), which increased the mechanical stress inside the micelles and allowed dimers to overcome the steric hindrance. Depending on the crossing angle, the resulting dimers also exhibited circular dichroism response on single-particle scale (Smith *et al.*, 2016).

Sphere NPs grafted with homopolymer ligands can self-assemble anisotopically as well. Kumacheva and coworkers demonstrated PS-modified AuNPs (~23 nm) could assemble into globules and NP chains in DMF/water, depending on the molecular weight of PS-SH and the solvent quality (Choueiri *et al.*, 2013). PS-50 K (50 kg/mol) grafted AuNPs would generate globules at C_w= 5 vol%, while PS-5 K (5 kg/mol) grafted AuNPs only remined as individual NPs or formed NP chains at C_w= 5 vol% and 15 vol% (**Fig. 5**(c)), respectively. The transition between these three nanostructures was reversible by altering water concentration (C_w). PGNP with a low molecular weight of PS ligands or under low C_w (below 5 vol%) likely formed individual NPs. A higher molecular weight of PS ligands and a low C_w favored the formation of the globules, whereas NP chains could be produced at a large C_w (15 vol%) regardless of the MW of PS ligands. The formation of different assemblies was attributed to the interplay between repulsive electrostatic interaction and attractive hydrophobic interaction. The size of globules correlated with the self-assemble time and C_w. The light scattering results showed that the hydrodynamic diameter of globules formed by AuNPs with PS-50 K at C_w= 7.5vol% gradually increased from 32.8 nm to 102.5 nm within 1 h. The formation of NP chains followed a step-growth mechanism with the average number of NPs per chain increased proportional with time. Such self-assembly behavior largely differs PGNPs from traditional isotropic NPs with polymer brushes. When polymer brushes are covalently linked on NP cores, those isotropic NPs would only aggregate irregularly. While the ligand-metal coordination is more dynamic, polymer ligands of those PGNPs can re-distribute on the surface of metal NPs to allow the collapse of those polymers anisotopically, particularly with a low grafting density of polymer ligands (Duan *et al.*, 2021).

Liz-Marzan *et al.* demonstrated the control self-assembly of PS-grafted AuNPs using an amphiphilic BCP surfactant (Sánchez-Iglesias *et al.*, 2012). The PGNPs were designed with an Au core (18 nm) grafted with PS_{509}-SH (53 kg/mol). In THF/water (80/20, vol) mixture, the collapse of PS ligands led to the self-assembly of AuNPs into clusters as indicated by the color change from red to pink along with the red-shifted of the LSPR peak from 540 nm to 565 nm (**Fig. 5**(d)). With long PS tethers, PGNPs aggregated irregularly to form clusters of PGNPs. The size of clusters continuously grew in the course of self-assembly and it reached 1–3 μm after 30 min. Those clusters eventually precipitated out after 1 day. The hydrophobicity-driven self-assembly was tuned by polymer-solvent interaction. The increase of the solvent quality to PS would trigger the dissociation of clusters into individual AuNPs. When replacing THF/water with pure THF, those cluster would redisperse with the recovery of the red color of AuNPs. When adding an amphiphilic BCP, *e.g.*, PS_{403}-PAA_{62}, during clustering, the further growth of nanoclusters could be prevented because hydrophobic interaction of PS tethers of PGNPs and the PS block of PS_{403}-PAA_{62} quenched the aggregation (**Fig. 5**(d)). Although the hydrophobicity-induced clustering of those PGNPs was reversible with varying the solvent quality, precise control of the NP numbers in each individual cluster was not satisfactory. In other words, clusters formed by solvent replacing were different at each time. A follow-up work by the same group solved such challenge by spatial confinement of assembled AuNPs into a porous silica shell (Sánchez-Iglesias *et al.*, 2018). Similarly, the clusters (7 ± 2 AuNPs) of PGNPs (AuNP 41 nm tethered by PS_{509}-SH) were prepared in THF/water and encapsulated into polymer micelle of PS_{403}-PAA_{62}. Those stable clusters coated by a mesoporous silica shell in water (**Fig. 5**(e)). The thickness of silica was 20 nm and the pore size was 4 nm. The permeability of the porous silica shell would render the removal of the BCP surfactant in THF while retaining PGNPs within the silica shell. After removal of the BCP, the hollow capsules with PGNPs were produced. The fully reversible transition between clusters and individual BCP could be easily triggered by altering the solvent quality. The capsules therefore offered the nanoconfinement to PGNPs to control the

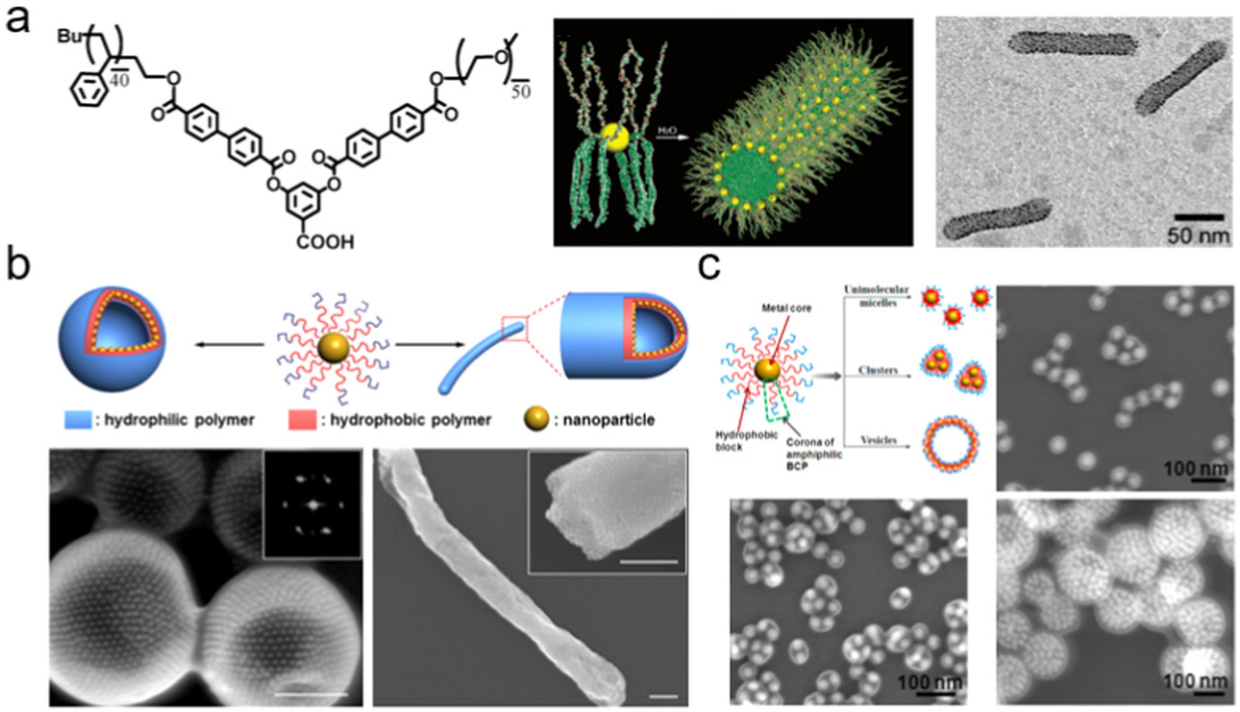

Fig. 6 (a) From left to right: chemical structure of PS_{40}-b-PEO_{50}; schematic illustration of the amphiphilicity driven self-assemble of AuNPs grafted by PS_{40}-b-PEO_{50}; TEM image showing the rod-like nanoarrays. Cited from (b) Scheme of amphiphilic BCP assisted self-assemble of AuNPs into vesicles or tubules and the SEM image of vesicles (inset: FFT) and tubule (scale bar = 200 nm). (c) Self-assemble of BCP grafted AuNPs into core-shell particles, clusters and vesicles with their corresponding SEM images. Cited from (a) Zubarev, E.R., Xu, J., Sayyad, A., Gibson, J.D., 2006. Amphiphilicity-driven organization of nanoparticles into discrete assemblies. J. Am. Chem. Soc. 128, 15098–15099. (b) He, J., Liu, Y., Babu, T., Wei, Z., Nie, Z., 2012. Self-assembly of inorganic nanoparticle vesicles and tubules driven by tethered linear block copolymers. J. Am. Chem. Soc. 134, 11342 –11345. (c) He, J., Huang, X., Li, Y.-C., *et al.*, 2013a. Self-assembly of amphiphilic plasmonic micelle-like nanoparticles in selective solvents. J. Am. Chem. Soc. 135, 7974–7984.

numbers of PGNPs within the clusters. The shift of the LSPR band from 572 nm to 542 nm was identical in multiple cycles of switching the water concentration from 50 vol% to 5 vol% (**Fig. 5**(e)).

While hydrophobicity-driven self-assembly of PGNPs tethered is powerful, the interaction is not directional. Polymer ligands uniformly distributed as the shell only provide isotropic interaction during self-assembly. The interparticle collapse of hydrophobic ligands is random as discussed in the previous examples where the clusters of PGNPs formed (Sánchez-Iglesias *et al.*, 2018, 2012). When co-assembling two or more types of PGNPs having different metal NP cores, other specific interactions, like hydrogen bonding, can be designed within PGNPs to guide the localized organization of different PGNPs. Macfarlane *et al.* demonstrated the use of the hydrogen bonding donor-acceptor interaction to induce the supramolecular recognition as inspired by spherical nucleic acids (Jones *et al.*, 2010; Liu *et al.*, 2016). PGNPs were grafted with PS-SH where the complementary hydrogen binding motifs including diaminopyridine (DAP) and thymine (Thy) were incorporated at the open end (exposed to the solvent) of PS ligands (Zhang *et al.*, 2016). The mixture of DAP-PS and Thy-PS modified AuNPs (20 nm) assembled rapidly in THF due to the paired hydrogen bonding between DAP and Thy. The assembled AuNPs formed macroscopically ordered lattices that precipitated out from THF. Since the hydrogen bonding of DAP-Thy was thermally liable, annealing at 55°C would cause the disassembly of PGNPs, along with the recovery of the original color and the LSPR peak. The dissociation temperature of DAP-Thy bonding in those nanostructures was different for all PGNPs. The characteristic disassembly temperature defined as melting temperature (T_m) increased with the size of AuNPs while it decreased with the longer PS ligands. The thermally annealed PGNP assemblies were body-centered cubic (bcc) packed regardless of the size of metal NP cores (Santos and Macfarlane, 2020).

Other than synthetic polymers, natural polymers, like proteins and DNA, can also been used to assemble metal NPs. Liu and Kotov recently demonstrated the co-assembly of AuNRs grafted by human islet amyloid polypeptide (hIAPP) with free hIAPP into chiral amyloid fibrils with chiro-optical response (Lu *et al.*, 2021). hIAPP-grafted AuNRs with the free hIAPP (1.3/2.7, mol) at solution formed long chains of NRs with end-to-end orientation. The fibers were left-handed helices with a pitch distance of 160 nm. Those one-dimensional assemblies had an intensive circular dichroism (CD) response of 2000 millidegrees. The CD spectra showed a red-shifted peak with a positive peak at 658 nm and a negative peak at 737 nm. The g-factor of PGNP assemblies increased dramatically to 0.12 at 661 nm which was 4600 times higher than that of hIAPP-grafted AuNRs in solution.

Other metal NPs, like magnetic cobalt NPs (CoNPs), have strong magnetic dipole-dipole interactions. Even in the presence of polymer ligands, those polymer-grafted NPs can assemble under external magnetic field. For example, ferromagnetic CoNPs

tethered by amine-terminated PS (5 kg/mol) could have strong magnetic dipole-dipole interaction even in the good solvent of polymers. In the presence of weak magnetic fields (100 mT), PS-grafted CoNPs underwent colloidal polymerization to form 1-D nanowires (Keng *et al.*, 2007; Kim *et al.*, 2010).

BCPs as Ligands to Guide the Self-Assembly of Metal NPs

The major issues on the self-assembly of PGNPs tethered with homopolymer ligands are two-fold: the unsatisfactory controllability and stability of assemblies. In case of hydrophobicity-driven self-assembly of PS-grafted AuNPs, clustering of those hydrophobic PGNPs is under kinetic control. Along with self-assembly, the size of clusters continuously increases till large clusters precipitate out from the solution. Moreover, those assembled nanostructures of PS-grafted AuNPs are only stable at a specific water concentration. In the absence of surfactants, *e.g.*, amphiphilic BCPs, collecting and isolating those assemblies are unlikely possible. Alternatively, amphiphilic BCPs if bound with AuNPs as surface ligands would offer an ideal solution to those challenges. While the hydrophobic block will provide a similar driving force for self-assembly, the hydrophilic block will enable the solubility of PGNPs and their assembled nanostructures. With more precise design of the BCP ligands in terms of their chemical composition and hydrophilic-to-hydrophobic ratio, much more sophisticated nanostructures of those PGNPs can be encountered as compared to that of homopolymer ligands.

The first example on self-assembly of PGNPs tethered with amphiphilic BCPs was reported by Zubarev *et al.* (2006) An V-shaped amphiphilic BCP of PS_{40}-*b*-PEO_{50} ($M_w = 8.2$ kg/mol, PDI = 1.1) with a COOH group at its focal point was used to modify AuNPs (2 nm) through the esterification between COOH and 4-mercaptophenol-capped AuNPs (**Fig. 6**(a)). Those PGNPs were soluble in the good solvent of PS_{40}-*b*-PEO_{50}, like THF. After adding water as a selective solvent, AuNPs grafted by PS_{40}-*b*-PEO_{50} could assemble to 1-D rods. Those rods had a diameter of 18.2 nm and a length of *ca.* 100 nm. AuNPs were found at the interface of the insoluble PS core and the water-soluble PEO shell, as a result of hydrophobicity driven spatial separation of the two blocks on the surface of AuNPs. The radius of the cylindrical nanostructure was 9 nm, comparable with the length of fully extended PS arms (10 nm). The size and the assembled morphology could be controlled by the solvent quality. Longer 1-D nanoarray with branches could be generated in DMF/water. The increase of the PGNP concentration in DMF would lead to the morphological transition from cylinders to vesicles. The size of metal NP cores was found be critical where AuNPs with a large diameter ($\sim$5 nm) grafted with PS_{40}-*b*-PEO_{50} did not self-assemble. To allow the reconformation of polymer chains, the chain length of the hydrophobic block should be significantly larger than the size of AuNPs.

Nie and coworkers later developed a more general self-assembly strategy of PGNPs tethered by amphiphilic BCPs (He *et al.*, 2012). The polymer ligands were designed with a short hydrophilic PEO block (2 kg/mol) and a hydrophobic PS block end with a thiol group. The molecular weight of the PS block varied from 5.7 kg/mol to 47.3 kg/mol to control the interparticle interaction. The self-assembly of PGNPs was carried through the film rehydration in which the PGNPs was first dried to form a thin film and then hydrated by sonication. After hydration, those PGNPs were found to form hollow vesicles and tubules (**Fig. 6**(b)). While the isotropic distribution of BCP ligands would form spherical core-shell NPs on the surface of AuNPs, the conformational rearrangement of grafted BCP ligands was proposed to minimize the interfacial energy of the hydrophobic PS with water. During the rehydration, AuNPs formed a highly ordered monolayer on the vesicular or tubular membranes. The hydrophilic PEO blocks were stretched out to stabilize the nanostructures and the PS blocks collapsed together in between AuNPs. The formation of vesicles was driven by the film rolling and reuniting that were highly determined by sonication condition. With a long PS chain and small AuNP core, the sonication did not provide enough driving force to rehydrate the film. It, therefore, had less thermodynamic control, particularly to correlate the outcomes of self-assembly with polymer structures.

In the classic self-assembly of amphiphilic BCPs using solvent exchange, it allows the relaxation of polymer chains at a much longer time domain, although true thermodynamic equilibrium cannot be reached. As compared to linear BCPs, PGNPs show much larger sizes and more complex chain conformation on the surface of metal NPs. As such, the assembly kinetics of PGNPs is slowed down significantly. As a follow-up study, Nie's group explored the self-assembly of similar PGNPs in the mixed solvent (He *et al.*, 2013a). With a reasonably low grafting density ($\sim$0.1 chains/nm^2) of BCPs, PGNPs consisting of Au cores and PEO_{45}-b-PS_x-SH shells were able to assemble in THF/water. The yielded self-assembly nanostructures of PGNPs were similar to that of linear BCPs. Using AuNPs with a diameter of 20 nm as an example, clear morphological transitions from core-shell NPs to clusters and eventually to vesicles were observed with the same AuNPs when the molecular weight of the PS block increased from 7 kg/mol to 49 kg/mol (**Fig. 6**(c)). Similar to linear BCPs, the average aggregation number (N_{agg}) or the number of PGNPs per assembly showed a clear power law dependence on the number of repeating units of the PS block. For 20 nm AuNPs, the N_{agg} was exponentially depended on N_{PS} in the order of 3.2 ($N_{agg} \sim N_{PS}^{3.2}$). The simulation studies form dissipative particle dynamics (DPD) suggested that a large enthalpic contribution of the PS blocks was critical to overcome the steric repulsion between the hydrated PEO blocks. The self-assembly of AuNPs would result in strong plasmonic coupling with large AuNPs ($\sim$40 nm). New plasmonic peaks in near infrared range (700–800 nm) were observed in those vesicles of 40 nm AuNPs that were of particular interest for biomedical applications.

The assembly can also be done through more dedicated control of solvent mixing, *e.g.*, under hydrodynamic flow in microfluidics. The fluid mixing conditions, *i.e.*, the flow rate (Q) to control the mixing of the two solvents, play a critical role in determining the assembly morphologies of PGNPs since they are kinetically slow. Using AuNRs modified by PEO_{45}-*b*-PS_{211} (23.9 kg/mol), the hydrodynamic flow controlled assembly could be carried out by focusing the THF solution of PGNPs between

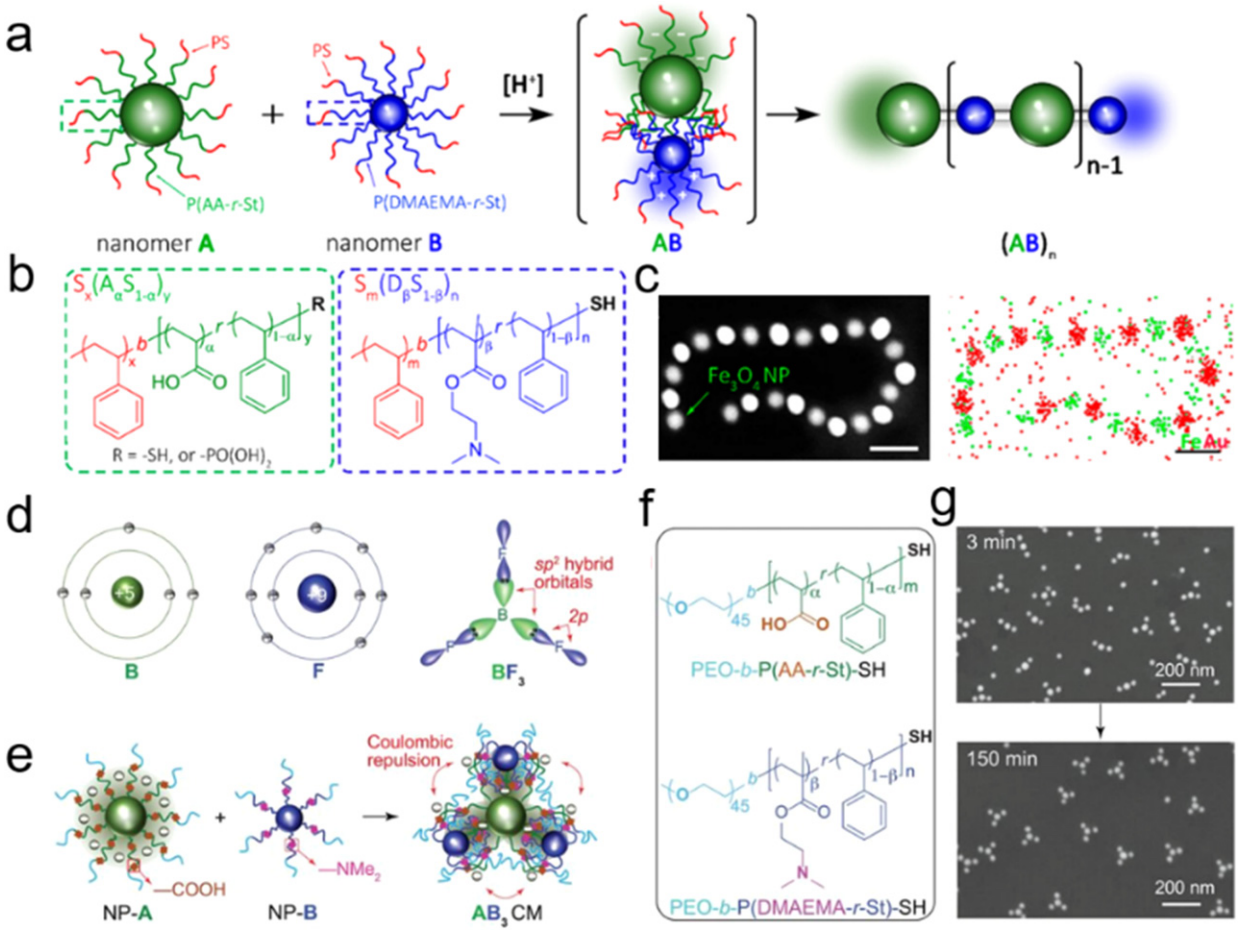

Fig. 7 (a) Schematics of binary AuNPs grafted with acid or base groups containing BCP ligand and their copolymerization into nanochains. (b) Chemical structure of acid and base group containing BCP ligands. (c) HAADF STEM and corresponding elemental mapping of nanochains prepared by alternating copolymerization of AuNPs and Fe_3O_4 NPs. (d) Schematic representation of boron (B) and fluoride (F) atoms and the structure of a sp^2-hybridized BF_3 molecule. (e) Scheme of the formation of AB_3-type nanostructure through directional binding NP-A and NP-B. (f) Chemical structure of PEO-b-P(AA-r-St) and PEO-b-P(DMAEMA-r-St). (g) SEM images showing the formation of AB_3-type nanostructures 3 min and 150 min after mixing NP-A and NP-B. Cited from Yi, C., Yang, Y., Nie, Z., 2019. Alternating copolymerization of inorganic nanoparticles. J. Am. Chem. Soc. 141, 7917 –7925. Yi, C., Liu, H., Zhang, S., *et al.*, 2020a. Self-limiting directional nanoparticle bonding governed by reaction stoichiometry. Science 369, 1369–1374.

two streams of water (He *et al.*, 2013c). With $Q_{THF} \ll Q_{water}$, the THF solution of PGNP was strongly focused and depleted quickly to mix with water, leading to the formation of AuNR supermicelles (< 100 nm). With $2.5 < Q_{water}/Q_{THF} < 7.5$, giant vesicles ($> 500$ nm) of AuNRs became the dominant products. The low focusing region allowed the slow diffusion and mixing of the two phases at the laminar flow interfaces. Those vesicles could not be generated under normal solvent mixing while the kinetic control in microfluidics was critical to produce such unique assemblies. The size of giant vesicles was variable in the broad range of 0.5–2 μm by tuning the flow rate of the two phases. Similarly, the hydrodynamic flow offered the kinetic control over spherical PGNPs (Moffitt, 2013; He *et al.*, 2013b; Coleman and Moffitt, 2018). With AuNPs (5 nm) grafted by PEO_{45}-*b*-PS_{455} (49.3 kg/mol), the size of vesicles prepared through the same method was controllable in the range of 100–600 nm by varying hydrodynamic flow conditions (He *et al.*, 2013b).

As aforementioned, hydrophobicity-driven self-assembly is less directional without anisotropic ligand distribution that may be controlled by ligand density or site-specific grafting. The alternative solution is to incorporate other directional interparticle interactions (*e.g.*, positive-negative charge attraction (Yi *et al.*, 2019) and hydrogen bond donor-acceptor (Zhang *et al.*, 2016)) that can differ the two types of PGNPs and introduce the another level of self-organization in the assemblies. Nie's group reported the periodic co-assembly of PGNPs having different sizes as a colloidal analogy of the perfect alternating sequence as Nylon-66 (Yi *et al.*, 2019). They utilized the paired attraction of oppositely charged NPs; *that is*, positively charged PGNPs only attracted negatively charged PGNPs while repulsed other positively charged PGNPs (**Fig. 7**(a)). The BCP ligands were designed as PS-*b*-poly(acrylic acid-*r*-styrene) (S_x ($A_\alpha S_{1-\alpha}$)$_y$) and PS-*b*-poly(N,N-dimethylaminoethyl methacrylate-*r*-styrene) (S_m ($D_\beta S_{1-\beta}$)$_n$) (**Fig. 7**(b)). The two BCPs had a protective PS block to provide the steric stabilization to PGNPs; while the other functional blocks

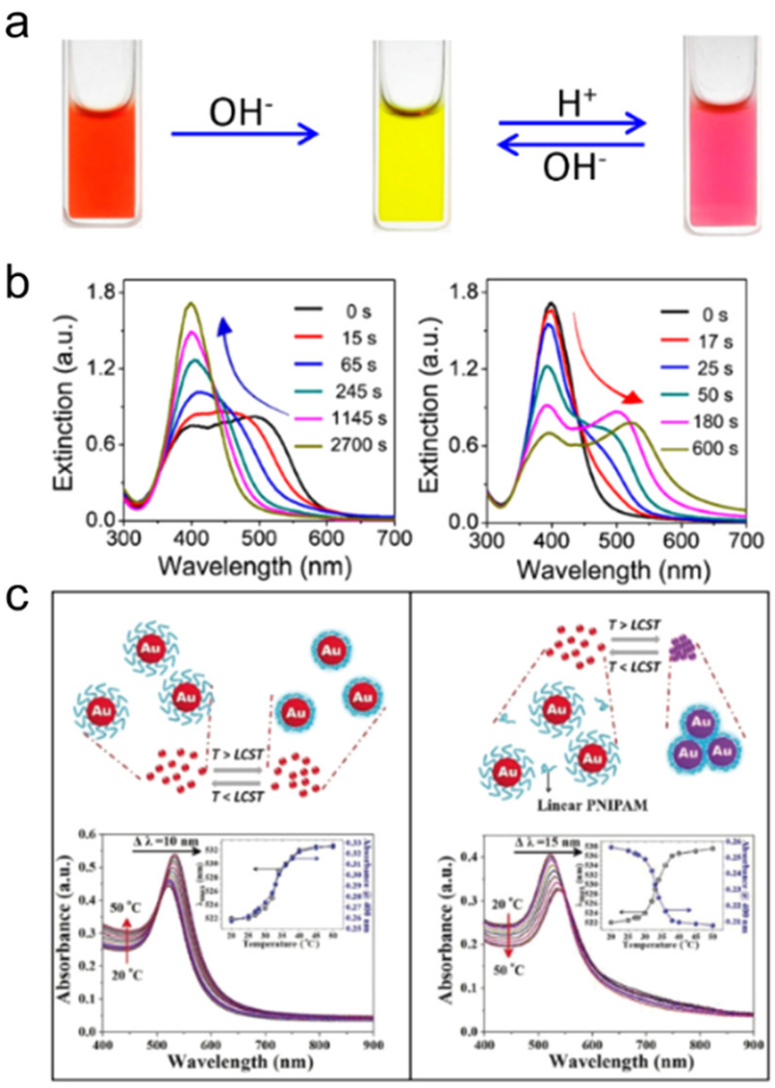

Fig. 8 (a) Images of initial, disassembled, and reassembled AgNPs. (b) UV–vis spectra of the dispersion of AgNP assemblies by adding NaOH and H_3PO_4. (c) Schematic illustration of the thermal responsive behavior of PNIPAM-capped AuNPs and the UV–vis spectra evolution with the change of temperature (left: no free PNIPAM; right: 0.081 mM free PNIPAM). Cited from Liu, L., Gao, Z., Jiang, B., *et al.*, 2018. Reversible assembly and dynamic plasmonic tuning of Ag nanoparticles enabled by limited ligand protection. Nano Lett. 18, 5312–5318. Chen, Y., Wang, Z., Harn, Y.W., *et al.*, 2019. Resolving optical and catalytic activities in thermoresponsive nanoparticles by permanent ligation with temperature-sensitive polymers. Angew. Chem. Int. Ed. 58, 11910–11917.

were random copolymers. The acidic COOH and basic tertiary amine (-NMe_2) groups would attract each other due to the opposite charge, leading to the formation of AB-type dimers. In the presence of acetic acid, simple mixing of binary NPs with carboxyl acid and tertiary amine would lead to the formation of chains with 100% A-B alternating sequence. The mechanism of such polymerization of NPs involved with a two-stage process as the electrostatic attraction-controlled oligomerization and diffusion-controlled polymerization. This method was able to extend to other metal or oxide NPs with various chemical composition, indicating the excellent generality. The alternating chains could be formed by different combinations as AgNPs or iron oxide (Fe_3O_4) NPs with AuNPs which were grafted with the negatively charged S_x $(A_\alpha S_{1-\alpha})_y$ and positively charged S_m $(D_\beta S_{1-\beta})_n$ (**Fig. 7**(c)), respectively.

Self-assembly of those binary PGNPs tethered by charged BCPs can be more precisely controlled through the balance of electrostatic interaction and steric repulsion. A more recent work from Nie's group developed the atom-bonding mimicking assembly using those binary PGNPs (**Fig. 7**(d)) (Yi *et al.*, 2020a). Binary NPs were first isotropically grafted with thiol-terminated PEO-*b*- (acrylic acid-*r*-styrene) [PEO-*b*-P(AA-*r*-St)] and PEO-*b*-poly(*N*,*N*-dimethylaminoethyl methacrylate-*r*-styrene) (PEO-*b*-P(DMAEMA-*r*-St)] denoted as the NP-A and NP-B (**Fig. 7**(e) and (f)). The two NP cores could be metallic (Au or Ag) or oxides (Fe_3O_4). Through stoichiometric mixing of NP-A and NP-B in THF, the neutralization reaction between acid and base in polymer ligands drove the formation of directional colloidal bonding analogous to the molecular bonding of AB_x (x = 1, 2, 3, 4, 5 and 6). The dynamic conformational change of the BCP

ligands allowed the formation of stoichiometric colloidal bonding of NP-A and NP-B. The self-assembly of NP-A and NP-B was self-limited. When the neutralization between acid and base groups completed, no further new bonds would form. The ratio x was determined by the reaction stoichiometry N_A/N_B, the ratio of the total number of acid groups on NP-A and base groups on NP-B that was adjusted by tuning the grafting density, polymer composition and NP size. For example, NP-A and NP-B were constructed by the combination of 36 nm AuNPs with PEO_{45}-*b*-$P(AA_{0.31}$-*r*-$St_{0.69})_{430}$ and 26 nm AuNPs and PEO_{45}-*b*-$P(DMAEMA_{0.31}$-*r*-$St_{0.69})_{244}$, respectively. With a N_A/N_B ration of ~2.8, AB_3-type nanostructures were generated after 150 min with a yield of *ca.* 80% (**Fig. 7**(g)). Since those colloidal AB_x building blocks have hydrophobic PS blocks, the programmable self-assemble of AB_x into hierarchical nanostructures could be further triggered by hydrophobicity. For example, AB_2-type linear nanostructures could form linear chain superstructures.

Responsive Self-Assembly of Metal Nanoparticles

Assembling PGNPs into nanostructure results in plasmon coupling that shifts or produces new plasmonic absorption peaks of metal NPs. Plasmon coupling is distance-sensitive, and its coupling strength decays exponentially with l/d, where l is the distance of adjacent NPs and d is the diameter of metal NPs (Jain *et al.*, 2007). With large metal NPs and short polymer chains, the strong plasmon coupling usually leads to the color change of plasmonic NPs. Since the interparticle gap is filled and controlled by polymer ligands, the distance of adjacent NPs l can be tuned by the physical state of polymers, like solvation and chain stretching. When increasing the solvation of polymer ligands as an example, it will increase the interparticle distance thus decrease the plasmon coupling strength. Among the examples discussed previously, (Sánchez-Iglesias *et al.*, 2018; Li *et al.*, 2015; He *et al.*, 2013a) PS-grafted AuNPs when assembled in THF/water had a red-shift plasmon peak while the plasmon peak could be recovered with the reverse titration of THF to solvate PS ligands. If grafting PGNPs with smart polymers that can change their physical properties in response to external stimuli, *e.g.*, pH, temperature, light and stress, one can design responsive assemblies of PGNPs. In couple with the color change, those responsive PGNP assembles can report the local change of polymer ligands more sensitively and visually.

PAA, for example, is a weak acid with its pKa of 4.5. Below its pKa, most of the carboxylic acid groups of PAA are protonated and PAA becomes water-insoluble. When grafting PAA on PGNPs, the assembly and disassembly of those PGNPs are pH-responsive. Yin and coworkers demonstrated the reversible and pH-responsive assemblies of AgNPs grafted with PAA (Liu *et al.*, 2018). When capped with PAA, the stability of AgNPs largely depends on electrostatic repulsion provided by deprotonated carboxylate. Using limited ligand protected growth, they first synthesized large PAA-capped AgNP assemblies (~165 nm) with a LSPR peak at 510 nm. Upon the addition of NaOH, the color of AgNP assemblies changed from red brown to yellow along with the shift of the LSPR peak to 400 nm. Subsequent addition of H_3PO_4 re-constructed the assembly by the protonation of carboxylate and the plasmonic coupling peak switched back to 510 nm and the color tuned from yellow to pink (**Fig. 8**(a) and (b)). The reversible assembly and disassembly of PAA-capped AgNPs were controlled by the surface charge density. The Zeta potential (ζ) of AgNPs increased from − 31 to − 57 mV upon the addition of 0.5 M NaOH solution, due to the deprotonation of PAA. This increased the electrostatic repulsion among AgNPs, leading to the disassembly of those large AgNP assemblies. The further protonation of PAA induced by the addition of H_3PO_4 would generate a reverse change of ζ from − 57 to − 6 mV, resulting in the reverse aggregation of those AgNPs. The similar design can be extended to humidity induced color switching of AgNPs using borate to deliver hydroxide reversibly (Liu *et al.*, 2019).

Song *et al.* (2011) reported the example of pH-responsive vesicles of PGNPs tethered with mixed polymer brushes. The mixed polymer brushes of PEO and PMMA were grafted on AuNPs (14 nm) using the combined grafting to and grafting from methods. 4-Vinylpyridine (4VP) as an ionizable group was introduced into the hydrophobic P(MMA-*r*-4VP) ligands. Those PGNPs tethered with PEO and P(MMA-*r*-4VP) assembled into vesicles through film rehydration. By decreasing pH from 7 to 5, the plasmonic vesicles deconstructed along with the blue-shift of the plasmon peak. The protonation of 4VP with strong electrostatic repulsion balanced out the hydrophobic interaction provided by the PMMA block, leading to the disruption of those plasmonic assemblies.

PNIPAM is a thermo-responsive polymer. Metal NPs grafted with PNIPAM can show temperature-responsive plasmonic color change because of the reversible hydration and dehydration of PNIPAM (Chen *et al.*, 2019; Maji *et al.*, 2016). When PNIPAM brushes reversibly collapse on the surface of metal NPs, the surface accessibility may also be regulated by polymer ligands as demonstrated by Lin's group (Chen *et al.*, 2019). Using the 21 β-CD with PAA-*b*-PNIPAM as a nanoreactor template, AuNPs could grow in the PAA domain while the PNIPAM remined as surface ligands. As-synthesized AuNPs had a diameter of 14.5 nm with a PNIPAM shell of 10.6 nm. When increasing the temperature from 20°C to 50°C, the thickness of PNIPAM shell shrinks to 5.8 nm with a red shift of LSPR peak from 522 nm to 532 nm (**Fig. 8**(c)). Above the lower critical solution temperature (LCST) the PNIPAM ligand collapsed on the surface of AuNPs without aggregation. However, when trace of free PNIPAM (~0.081 mM) was deliberately added into the PNIPAM-grafted AuNPs solution (1 mg/mL), aggregation of AuNPs was observed upon heating to 50°C with the SPR peak red shift by 15 nm (**Fig. 8**(c)). Free PNIPAM was found to act as a physical cross-linker to aggerate PNIPAM-grafted AuNPs. The collapse of PNPMA ligands on the surface of AuNPs had a profound effect on the catalytic activity of AuNPs. Using the reduction of 4-nitrophenol, those PNIPAM-grafted AuNPs showed an unconventional anti-Arrhenius-type behavior above the LCST of PNIPAM. Increasing temperature would cause the increased diffusion rate of reaction; and, at the same time, the shrinkage of the PNIPAM shell limited the accessibility of AuNPs. The two effects had an opposite impact to the reaction rate constant since the collapsed PNIPAM would hinder the diffusion of reactants to the surface of AuNPs. Therefore, the rate

constant decreased first from 25°C to 37.5°C) and then increased from 37.5°C to 50°C. In the follow-up study, Lin's group also developed light-responsive PGNPs grafted by poly(7-methylacryloyloxy-4-methylcoumarin) (PMAMC) (Chen *et al.*, 2018). The coumarin moieties in PMAMC is known for the (2 + 2) photodimerization. PMAMC-grafted AuNPs would aggregate when exposing to 365 nm UV light to drive the photodimerization of coumarin; while, they disassembled when irradiated with 254 nm deep UV to trigger the photocleavage.

Responsive assemblies of PGNPs can be achieved in solid state using stress as an external stimulus. The chains of AuNPs formed by adding electrolytes usually show very strong plasmonic coupling therefore the change of their color. Yin and coworkers demonstrated the disassembly of those chains of AuNPs under mechanical stretching or compressing (Han *et al.*, 2014). PVP-grafted AuNP chains could be dispersed in the PVP film where the color was deep blue due to the plasmon coupling between AuNPs. When compressing the film between two glasses, the color immediately changed from blue to red. The mechanical pull of the AuNP chain would increase the interparticle distance and thus decrease the plasmon coupling of adjacent NPs. As compared to organic mechanophore that are used to report the mechanic deformation of polymers, (Davis *et al.*, 2009) the assembled nanostructures of PGNPs are more robust in terms of their photo- and chemo-stability.

Summary

In this article, we summarize recent advances of PGNPs with a broad coverage on control synthesis, ligand exchange and their self-assembly. The marriage of polymer ligands with metal NPs serves as a new tool to create a novel class of building blocks as PGNPs with improved stability, tunable surface energy and controllable interparticle interactions. Starting with the binding motifs of polymer ligands, the design of polymer ligands through three different methods is discussed. We compared the binding strength of the anchoring groups (-SH *vs*. NHC) and the grafting methods (grafting to and grafting from) for different types of polymer ligands. Recent examples on template syntheses of PGNPs covalently grafted with polymers were highlighted. We discussed the isotropic-to-anisotropic transition of the surface patterning of PGNPs with a particular focus on anisotropic surface pattering of metal NPs. A few new methods including site-selective grafting and phase segregation-driven symmetry-broken grafting of PGNPs were also reviewed. Their potentials in hierarchical self-assembly as unique colloidal molecules were featured. Polymer ligands as an efficient way to vary the surface energy and balance the interparticle interaction could guide the self-assembly of those PGNPs. The self-assembly of PGNPs grafted by homopolymer or BCP ligands was accounted along with how self-assembly of PGNPs controls over the plasmon coupling of metal NPs. We also elaborated very recent studies on the hierarchical assembly of PGNPs having different metal NPs. The responsive self-assembly of PGNPs grafted with smart polymers was included with examples on various stimuli-responsive plasmonic nanostructures at the end.

Self-assembly of PGNPs is undoubtedly exciting with tremendous progress in the past decade. However, there still lacks precise control of building blocks themselves, in terms of their ligand density, surface patterning of polymer ligands and variation of metal NP cores. As closely related to the surface chemistry of metal NPs, the fundamental measurement on the kinetics of ligand exchange and the dynamic of surface ligands needs continuous effort. Since the surface of metal NPs is not well-defined as that of single crystals or metal nanoclusters, the development of new spectroscopical tools is desired to quantitatively study the dynamic behavior of polymer ligands, *e.g.*, the ligand exchange kinetics of polymer ligands *vs*. capping ligands of metal NPs, and the exchange kinetics of polymer ligands *vs*. polymer ligands, as demonstrated in previous NMR studies of ligand exchange reactions on quantum dots (Knauf *et al.*, 2016; Chambrier *et al.*, 2015). As one of the dynamic properties of PGNPs, the detachment and mobility of thiol-ended surface ligands on metal NPs has been previously reported in SAMs (Schönenberger *et al.*, 1995). Similar surface dynamics of polymer ligands has been found to be critical in tuning the surface patterning of metal NPs (Yang *et al.*, 2021; Galati *et al.*, 2020). We believe that, gaining those physicochemical parameters is fundamentally important to better understand the isotropic-to-anisotropic transition of polymer ligands and further engineer the hierarchical self-assembly outcomes of PGNPs. The synergies of polymers and metal NPs as integrated in PGNPs will bring ample opportunities to explore the intriguing applications of metal NPs in self-assembly, sensing, catalysis, and optics.

References

Bain, C.D., Troughton, E.B., Tao, Y.T., *et al.*, 1989. Formation of monolayer films by the spontaneous assembly of organic thiols from solution onto gold. J. Am. Chem. Soc. 111, 321–335.

Bakker, A., Freitag, M., Kolodzeiski, E., *et al.*, 2020. An electron-rich cyclic (Alkyl) (Amino) carbene on Au (111), Ag (111), and Cu (111) surfaces. Angew. Chem. Int. Ed. 59, 13643–13646.

Brust, M., Walker, M., Bethell, D., Schiffrin, D.J., Whyman, R., 1994. Synthesis of thiol-derivatised gold nanoparticles in a two-phase liquid – Liquid system. J. Chem. Soc. Chem. Commun. 801–802.

Chambrier, I., Banerjee, C., Remiro-Buenamañana, S., *et al.*, 2015. Synthesis of porphyrin–CdSe quantum dot assemblies: Controlling ligand binding by substituent effects. Inorg. Chem. 54, 7368–7380.

Chen, Q., Bae, S.C., Granick, S., 2011. Directed self-assembly of a colloidal kagome lattice. Nature 469, 381–384.

Chen, T., Yang, M., Wang, X., Tan, L.H., Chen, H., 2008. Controlled assembly of eccentrically encapsulated gold nanoparticles. J. Am. Chem. Soc. 130, 11858–11859.

Chen, Y., Wang, Z., He, Y., *et al.*, 2018. Light-enabled reversible self-assembly and tunable optical properties of stable hairy nanoparticles. Proc. Natl. Acad. Sci. USA 115, E1391–E1400.

Chen, Y., Wang, Z., Harn, Y.W., *et al.*, 2019. Resolving optical and catalytic activities in thermoresponsive nanoparticles by permanent ligation with temperature-sensitive polymers. Angew. Chem. Int. Ed. 58, 11910–11917.
Cheng, L., Liu, A., Peng, S., Duan, H., 2010. Responsive plasmonic assemblies of amphiphilic nanocrystals at oil – Water interfaces. ACS Nano 4, 6098–6104.
Choueiri, R.M., Klinkova, A., Thérien-Aubin, H.s., Rubinstein, M., Kumacheva, E., 2013. Structural transitions in nanoparticle assemblies governed by competing nanoscale forces. J. Am. Chem. Soc. 135, 10262–10265.
Choueiri, R.M., Galati, E., Thérien-Aubin, H., *et al.*, 2016. Surface patterning of nanoparticles with polymer patches. Nature 538, 79–83.
Coleman, B.R., Moffitt, M.G., 2018. Amphiphilic INorganic Nanoparticles With Mixed Polymer Brush Layers Of Variable Composition: Bridging The Paradigms Of Block Copolymer And Nanoparticle Self-assembly. Chem. Mater. 30, 2474–2482.
Corbierre, M.K., Cameron, N.S., Lennox, R.B., 2004. Polymer-stabilized gold nanoparticles with high grafting densities. Langmuir 20, 2867–2873.
Crudden, C.M., Horton, J.H., Ebralidze, I.I., *et al.*, 2014. Ultra stable self-assembled monolayers of N-heterocyclic carbenes on gold. Nat. Chem. 6, 409–414.
Davis, D.A., Hamilton, A., Yang, J., *et al.*, 2009. Force-induced activation of covalent bonds in mechanoresponsive polymeric materials. Nature 459, 68–72.
Delong, R.K., Reynolds, C.M., Malcolm, Y., *et al.*, 2010. Functionalized gold nanoparticles for the binding, stabilization, and delivery of therapeutic DNA, RNA, and other biological macromolecules. Nanotechnol. Sci. Appl. 3, 53–63.
DeVries, G.A., Brunnbauer, M., Hu, Y., *et al.*, 2007. Divalent metal nanoparticles. Science 315, 358–361.
Duan, H., Luo, Q., Wei, Z., Lin, Y., He, J., 2021. Symmetry-broken patches on gold nanoparticles through deficient ligand exchange. ACS Macro Lett. 10, 786–790.
Duan, H., Yang, Y., Zhang, Y., *et al.*, 2020. What is next in polymer-grafted plasmonic nanoparticles? Giant 4. 100033.
Ebeling, B., Vana, P., 2013. RAFT-polymers with single and multiple trithiocarbonate groups as uniform gold-nanoparticle coatings. Macromolecules 46, 4862–4871.
Engel, S., Fritz, E.-C., Ravoo, B.J., 2017. New trends in the functionalization of metallic gold: from organosulfur ligands to N-heterocyclic carbenes. Chem. Soc. Rev. 46, 2057–2075.
Frens, G., 1973. Controlled nucleation for the regulation of the particle size in monodisperse gold suspensions. Nat. Phys. Sci. 241, 20–22.
Gal, N., Schroffenegger, M., Reimhult, E., 2018. Stealth nanoparticles grafted with dense polymer brushes display adsorption of serum protein investigated by isothermal titration calorimetry. J. Phys. Chem. B 122, 5820–5834.
Galati, E., Tao, H., Rossner, C., Zhulina, E.B., Kumacheva, E., 2020. Morphological transitions in patchy nanoparticles. ACS Nano 14, 4577–4584.
Gao, J., Huang, X., Liu, H., Zan, F., Ren, J., 2012a. Colloidal stability of gold nanoparticles modified with thiol compounds: Bioconjugation and application in cancer cell imaging. Langmuir 28, 4464–4471.
Gao, C., Vuong, J., Zhang, Q., Liu, Y., Yin, Y., 2012b. One-step seeded growth of Au nanoparticles with widely tunable sizes. Nanoscale 4, 2875–2878.
Goulet, P.J.G., Bourret, G.R., Lennox, R.B., 2012. Facile phase transfer of large, water-soluble metal nanoparticles to nonpolar solvents. Langmuir 28, 2909–2913.
Grzelczak, M., Sánchez-Iglesias, A., Rodríguez-González, B., *et al.*, 2008. Influence of iodide ions on the growth of gold nanorods: Tuning tip curvature and surface plasmon resonance. Adv. Funct. Mater. 18, 3780–3786.
Grzelczak, M., Sánchez-Iglesias, A., Mezerji, H.H., *et al.*, 2012. Steric hindrance induces crosslike self-assembly of gold nanodumbbells. Nano Lett. 12, 4380–4384.
Häkkinen, H., 2012. The gold–sulfur interface at the nanoscale. Nat. Chem. 4, 443–455.
Han, S.W., Lee, S.J., Kim, K., 2001. Self-assembled monolayers of aromatic thiol and selenol on silver: Comparative study of adsorptivity and stability. Langmuir 17, 6981–6987.
Han, X., Liu, Y., Yin, Y., 2014. Colorimetric stress memory sensor based on disassembly of gold nanoparticle chains. Nano Lett. 14, 2466–2470.
He, J., Liu, Y., Babu, T., Wei, Z., Nie, Z., 2012. Self-assembly of inorganic nanoparticle vesicles and tubules driven by tethered linear block copolymers. J. Am. Chem. Soc. 134, 11342–11345.
He, J., Wang, L., Wei, Z., *et al.*, 2013b. Vesicular self-assembly of colloidal amphiphiles in microfluidics. ACS Appl. Mater. Interfaces 5, 9746–9751.
He, J., Wei, Z., Wang, L., *et al.*, 2013c. Hydrodynamically driven self-assembly of giant vesicles of metal nanoparticles for remote-controlled release. Angew. Chem. Int. Ed. 125, 2523–2528.
He, J., Huang, X., Li, Y.-C., *et al.*, 2013a. Self-assembly of amphiphilic plasmonic micelle-like nanoparticles in selective solvents. J. Am. Chem. Soc. 135, 7974–7984.
Jain, P.K., Huang, W., El-Sayed, M.A., 2007. On the universal scaling behavior of the distance decay of plasmon coupling in metal nanoparticle pairs: A plasmon ruler equation. Nano Lett. 7, 2080–2088.
Jana, N.R., Gearheart, L., Murphy, C.J., 2001. Seeding growth for size control of 5 – 40 nm diameter gold nanoparticles. Langmuir 17, 6782–6786.
Jones, M.R., Macfarlane, R.J., Lee, B., *et al.*, 2010. DNA-nanoparticle superlattices formed from anisotropic building blocks. Nat. Mater. 9, 913–917.
Kao, J., Bai, P., Chuang, V.P., *et al.*, 2012. Nanoparticle assemblies in thin films of supramolecular nanocomposites. Nano Lett. 12, 2610–2618.
Keng, P.Y., Shim, I., Korth, B.D., Douglas, J.F., Pyun, J., 2007. Synthesis and self-assembly of polymer-coated ferromagnetic nanoparticles. ACS Nano 1, 279–292.
Kim, A., Zhou, S., Yao, L., *et al.*, 2019. Tip-patched nanoprisms from formation of ligand islands. J. Am. Chem. Soc. 141, 11796–11800.
Kim, B.J., Bang, J., Hawker, C.J., Kramer, E.J., 2006. Effect of areal chain density on the location of polymer-modified gold nanoparticles in a block copolymer template. Macromolecules 39, 4108–4114.
Kim, B.Y., Shim, I.-B., Araci, Z.O., *et al.*, 2010. Synthesis and colloidal polymerization of ferromagnetic Au – Co nanoparticles into Au – Co3O4 nanowires. J. Am. Chem. Soc. 132, 3234–3235.
Knauf, R.R., Lennox, J.C., Dempsey, J.L., 2016. Quantifying ligand exchange reactions at CdSe nanocrystal surfaces. Chem. Mater. 28, 4762–4770.
Koczkur, K.M., Mourdikoudis, S., Polavarapu, L., Skrabalak, S.E., 2015. Polyvinylpyrrolidone (PVP) in nanoparticle synthesis. Dalton Trans. 44, 17883–17905.
Kyrychenko, A., Korsun, O.M., Gubin, I.I., Kovalenko, S.M., Kalugin, O.N., 2015. Atomistic simulations of coating of silver nanoparticles with poly(vinylpyrrolidone) oligomers: Effect of oligomer chain length. J. Phys. Chem. C 119, 7888–7899.
Larson, T.A., Joshi, P.P., Sokolov, K., 2012. Preventing protein adsorption and macrophage uptake of gold nanoparticles via a hydrophobic shield. ACS Nano 6, 9182–9190.
Lavrich, D.J., Wetterer, S.M., Bernasek, S.L., Scoles, G., 1998. Physisorption and chemisorption of alkanethiols and alkyl sulfides on Au (111). J. Phys. Chem. B 102, 3456–3465.
Leff, D.V., Brandt, L., Heath, J.R., 1996. Synthesis and characterization of hydrophobic, organically-soluble gold nanocrystals functionalized with primary amines. Langmuir 12, 4723–4730.
Li, W., Liu, S., Deng, R., Zhu, J., 2011. Encapsulation of nanoparticles in block copolymer micellar aggregates by directed supramolecular assembly. Angew. Chem. Int. Ed. 50, 5865–5868.
Li, W., Kanyo, I., Kuo, C.-H., Thanneeru, S., He, J., 2015. pH-programmable self-assembly of plasmonic nanoparticles: Hydrophobic interaction versus electrostatic repulsion. Nanoscale 7, 956–964.
Liang, R., Xu, J., Deng, R., *et al.*, 2014. Assembly of polymer-tethered gold nanoparticles under cylindrical confinement. ACS Macro Lett. 3, 486–490.
Liu, B., Thanneeru, S., Lopes, A., *et al.*, 2017. Surface engineering of spherical metal nanoparticles with polymers toward selective asymmetric synthesis of nanobowls and janus-type dimers. Small 13. 1700091.
Liu, K., Nie, Z., Zhao, N., *et al.*, 2010. Step-growth polymerization of inorganic nanoparticles. Science 329, 197–200.
Liu, L., Gao, Z., Jiang, B., *et al.*, 2018. Reversible assembly and dynamic plasmonic tuning of Ag nanoparticles enabled by limited ligand protection. Nano Lett. 18, 5312–5318.
Liu, L., Aleisa, R., Zhang, Y., *et al.*, 2019. Dynamic color-switching of plasmonic nanoparticle films. Angew. Chem. Int. Ed. 131, 16453–16459.
Liu, T., Thierry, B., 2012. A solution to the PEG dilemma: Efficient bioconjugation of large gold nanoparticles for biodiagnostic applications using mixed layers. Langmuir 28, 15634–15642.

Liu, W., Tagawa, M., Xin, H.L., *et al.*, 2016. Diamond family of nanoparticle superlattices. Science 351, 582–586.
Liu, Y., Wang, J., Zhang, M., Li, H., Lin, Z., 2020. Polymer-ligated nanocrystals enabled by nonlinear block copolymer nanoreactors: Synthesis, properties, and applications. ACS Nano 14, 12491–12521.
Lowe, A.B., Sumerlin, B.S., Donovan, M.S., McCormick, C.L., 2002. Facile preparation of transition metal nanoparticles stabilized by well-defined (Co)polymers synthesized via aqueous reversible addition-fragmentation chain transfer polymerization. J. Am. Chem. Soc. 124, 11562–11563.
Lu, J., Xue, Y., Bernardino, K., *et al.*, 2021. Enhanced optical asymmetry in supramolecular chiroplasmonic assemblies with long-range order. Science 371, 1368–1374.
Maji, S., Cesur, B., Zhang, Z., De Geest, B.G., Hoogenboom, R., 2016. Poly(N-isopropylacrylamide) coated gold nanoparticles as colourimetric temperature and salt sensors. Polym. Chem. 7, 1705–1710.
Moffitt, M., McMahon, L., Pessel, V., Eisenberg, A., 1995. Size control of nanoparticles in semiconductor-polymer composites. 2. Control via sizes of spherical ionic microdomains in styrene-based diblock ionomers. Chem. Mater. 7, 1185–1192.
Moffitt, M.G., 2013. Self-assembly of polymer brush-functionalized inorganic nanoparticles: from hairy balls to smart molecular mimics. J. Phys. Chem. Lett. 4, 3654–3666.
Mössmer, S., Spatz, J.P., Möller, M., *et al.*, 2000. Solution behavior of poly(styrene)-block-poly(2-vinylpyridine) micelles containing gold nanoparticles. Macromolecules 33, 4791–4798.
Mout, R., Moyano, D.F., Rana, S., Rotello, V.M., 2012. Surface functionalization of nanoparticles for nanomedicine. Chem. Soc. Rev. 41, 2539–2544.
Narouz, M.R., Osten, K.M., Unsworth, P.J., *et al.*, 2019. N-heterocyclic carbene-functionalized magic-number gold nanoclusters. Nat. Chem. 11, 419–425.
Nie, Z., Fava, D., Kumacheva, E., *et al.*, 2007. Self-assembly of metal–polymer analogues of amphiphilic triblock copolymers. Nat. Mater. 6, 609–614.
Nuß, S., Böttcher, H., Wurm, H., Hallensleben, M.L., 2001. Gold nanoparticles with covalently attached polymer chains. Angew. Chem. Int. Ed. 40, 4016–4018.
Ohno, K., Koh, K.-m., Tsujii, Y., Fukuda, T., 2002. Synthesis of gold nanoparticles coated with well-defined, high-density polymer brushes by surface-initiated living radical polymerization. Macromolecules 35, 8989–8993.
Ojea-Jiménez, I., Puntes, V., 2009. Instability of cationic gold nanoparticle bioconjugates: The role of citrate ions. J. Am. Chem. Soc. 131, 13320–13327.
Pang, X., He, Y., Jung, J., Lin, Z., 2016. 1D nanocrystals with precisely controlled dimensions, compositions, and architectures. Science 353, 1268–1272.
Pang, X., Zhao, L., Han, W., Xin, X., Lin, Z., 2013. A general and robust strategy for the synthesis of nearly monodisperse colloidal nanocrystals. Nat. Nanotechnol. 8, 426–431.
Roth, P.J., Theato, P., 2008. Versatile synthesis of functional gold nanoparticles: Grafting polymers from and onto. Chem. Mater. 20, 1614–1621.
Sánchez-Iglesias, A., Grzelczak, M., Altantzis, T., *et al.*, 2012. Hydrophobic interactions modulate self-assembly of nanoparticles. ACS Nano 6, 11059–11065.
Sánchez-Iglesias, A., Claes, N., Solís, D.M., *et al.*, 2018. Reversible clustering of gold nanoparticles under confinement. Angew. Chem. Int. Ed. 130, 3237–3240.
Santos, P.J., Macfarlane, R.J., 2020. Reinforcing supramolecular bonding with magnetic dipole interactions to assemble dynamic nanoparticle superlattices. J. Am. Chem. Soc. 142, 1170–1174.
Schönenberger, C., Jorritsma, J., Sondag-Huethorst, J., Fokkink, L., 1995. Domain structure of self-assembled alkanethiol monolayers on gold. J. Phys. Chem. 99, 3259–3271.
Shaw, D.J., 1980. Introduction to Colloid and Surface Chemistry. Butterworths.
Smith, K.W., Zhao, H., Zhang, H., *et al.*, 2016. Chiral and achiral nanodumbbell dimers: The effect of geometry on plasmonic properties. ACS Nano 10, 6180–6188.
Song, J., Cheng, L., Liu, A., *et al.*, 2011. Plasmonic vesicles of amphiphilic gold nanocrystals: self-assembly and external-stimuli-triggered destruction. J. Am. Chem. Soc. 133, 10760–10763.
Spatz, J.P., Mössmer, S., Hartmann, C., *et al.*, 2000. Ordered deposition of inorganic clusters from micellar block copolymer films. Langmuir 16, 407–415.
Sun, Y., Yin, Y., Mayers, B.T., Herricks, T., Xia, Y., 2002. Uniform silver nanowires synthesis by reducing AgNO3 with ethylene glycol in the presence of seeds and poly(vinyl pyrrolidone). Chem. Mater. 14, 4736–4745.
Tadros, T., 2013. Steric stabilization. In: Tadros, T. (Ed.), Encyclopedia of Colloid and Interface Science. Berlin, Heidelberg: Springer Berlin Heidelberg, pp. 1048–1049.
Thanneeru, S., Ayers, K.M., Anuganti, M., *et al.*, 2020. N-Heterocyclic carbene-ended polymers as surface ligands of plasmonic metal nanoparticles. J. Mater. Chem. C 8, 2280–2288.
Wang, B., Li, B., Zhao, B., Li, C.Y., 2008. Amphiphilic janus gold nanoparticles via combining "Solid-State Grafting-to" and "Grafting-from" methods. J. Am. Chem. Soc. 130, 11594–11595.
Wang, B., Li, B., Dong, B., Zhao, B., Li, C.Y., 2010. Homo-and hetero-particle clusters formed by janus nanoparticles with bicompartment polymer brushes. Macromolecules 43, 9234–9238.
Wang, F., Cheng, S., Bao, Z., Wang, J., 2013. Anisotropic overgrowth of metal heterostructures induced by a site-selective silica coating. Angew. Chem. Int. Ed. 125, 10534–10538.
Wang, Y.-X., Li, Y., Qiao, S.-H., *et al.*, 2021. Polymers via reversible addition–fragmentation chain transfer polymerization with high thiol end-group fidelity for effective grafting-to gold nanoparticles. J. Phys. Chem. Lett. 12, 4713–4721.
Weidner, T., Baio, J.E., Mundstock, A., *et al.*, 2011. NHC-based self-assembled monolayers on solid gold substrates. Aust. J. Chem. 64, 1177–1179.
Westmoreland, D.E., López-Arteaga, R., Weiss, E.A., 2020. N-heterocyclic carbenes as reversible exciton-delocalizing ligands for photoluminescent quantum dots. J. Am. Chem. Soc. 142, 2690–2696.
Xu, X., Rosi, N.L., Wang, Y., Huo, F., Mirkin, C.A., 2006. Asymmetric functionalization of gold nanoparticles with oligonucleotides. J. Am. Chem. Soc. 128, 9286–9287.
Yamamoto, Y., Nishihara, H., Aramaki, K., 1993. Self-assembled layers of alkanethiols on copper for protection against corrosion. J. Electrochem. Soc. 140, 436–443.
Yang, Y., Yi, C., Duan, X., *et al.*, 2021. Block-random copolymer-micellization-mediated formation of polymeric patches on gold nanoparticles. J. Am. Chem. Soc. 143, 5060–5070.
Yi, C., Yang, Y., Nie, Z., 2019. Alternating copolymerization of inorganic nanoparticles. J. Am. Chem. Soc. 141, 7917–7925.
Yi, C., Yang, Y., Liu, B., He, J., Nie, Z., 2020b. Polymer-guided assembly of inorganic nanoparticles. Chem. Soc. Rev. 49, 465–508.
Yi, C., Liu, H., Zhang, S., *et al.*, 2020a. Self-limiting directional nanoparticle bonding governed by reaction stoichiometry. Science 369, 1369–1374.
Zhang, J., Santos, P.J., Gabrys, P.A., *et al.*, 2016. Self-assembling nanocomposite tectons. J. Am. Chem. Soc. 138, 16228–16231.
Zhang, L., He, R., Gu, H.-C., 2006. Oleic acid coating on the monodisperse magnetite nanoparticles. Appl. Surf. Sci. 253, 2611–2617.
Zhang, L., Wei, Z., Meng, M., Ung, G., He, J., 2020. Do polymer ligands block the catalysis of metal nanoparticles? Unexpected importance of binding motifs in improving catalytic activity. J. Mater. Chem. A 8, 15900–15908.
Zhang, L., Wei, Z., Thanneeru, S., *et al.*, 2019. A polymer solution to prevent nanoclustering and improve the selectivity of metal nanoparticles for electrocatalytic CO_2 reduction. Angew. Chem. Int. Ed. 131, 15981–15987.
Zubarev, E.R., Xu, J., Sayyad, A., Gibson, J.D., 2006. Amphiphilicity-driven organization of nanoparticles into discrete assemblies. J. Am. Chem. Soc. 128, 15098–15099.